

A Sequence Stratigraphic approach to interpreting the $\delta^{13}\text{C}$ record using an Early Cambrian Carbonate Platform

Thesis submitted in accordance with the requirements of the University of
Adelaide for an Honours Degree in Geology

Claire Marie Kenefick

November 2013



THE UNIVERSITY
of ADELAIDE

TITLE

A Sequence Stratigraphic approach to interpreting the $\delta^{13}\text{C}$ record using an Early Cambrian Carbonate Platform

RUNNING TITLE

Sequence Stratigraphic approach to interpreting the $\delta^{13}\text{C}$ record

ABSTRACT

The Early Cambrian Wilkawillina Platform displays a continuous platform to basin facies that enables physical time surfaces to be used to compare roughly synchronous $\delta^{13}\text{C}$ values of carbonates to test their lateral variation in range. The two sections measured showed a progression from shallow water deposition of the Woodendinna Dolomite to deeper water deposition of the Oraparinna Shale in the basin while biostromes of *Archaeocyatha* developed on the shelf. Using a sequence stratigraphic approach, the sections were correlated using the time significant sequence boundaries shared between the two sections. Correlated by the sequence boundaries, stable isotopes ($\delta^{13}\text{C}$ and $\delta^{18}\text{O}$) were then compared and found to be out of phase with each other. A chronostratigraphic diagram shows that carbonate deposition is not continuous over time and therefore, the $\delta^{13}\text{C}$ record is episodic. This approach emphasises the punctuated nature of the record and the predominance of depositional hiatus in sections, while previous chemostratigraphic studies have assumed the $\delta^{13}\text{C}$ record to be largely continuous through time when making correlations.

KEYWORDS

Sequence Stratigraphy, $\delta^{13}\text{C}$ record, carbonate platforms, Wilkawillina Platform, Early Cambrian, stratigraphic correlation, chemostratigraphy.

TABLE OF CONTENTS

Title.....	2
Running title	2
Abstract.....	2
Keywords.....	2
List of Figures and Tables	4
Introduction	5
Geological Setting	13
Methods	17
Observations and Results	18
Stratigraphic Sections	18
Sequence Stratigraphy	23
Physical stratigraphic model.....	27
Stable Isotopes.....	29
Discussion.....	32
Conclusions	40
Acknowledgments	42
References	43
Appendix A: Methods	46
Appendix B: Supplementary Results.....	46

LIST OF FIGURES AND TABLES

Figure 1: Sequence boundaries separate lithologies, facies, and stable isotope signals; even if previously correlated. Only the younger stratigraphy lying above the SB can be correlated, and the older stratigraphy below, but never the stratigraphy from either side of the SB. Hence only $\delta^{13}\text{C}$ values from the same side of the boundary can be correlated.	12
Figure 2: Location Map for the Wilkawillina Platform, Flinders Ranges, South Australia.	13
Figure 3: (a) Section 1 represents the slope to basin facies of the Wilkawillina platform. (b) Section 2 represents the slope to platformal facies.	21
Figure 4: Evidence of diagenetic alteration. (a) Recrystallised oolite of the Woodendinna Dolomite stained with Alizarin red S, note the meteoric calcite cements infilling pore spaces around ooids (equant calcite; white arrow, XPL). (b) Recrystallised Bunkers Sandstone stained with Alizarin red S, calcite (red) and dolomite (yellow arrows) fill pore spaces in an interlocking pattern with quartz grains (XPL). (c) Red-dashed line shows the dolomitic front of discolouration at a karst surface. (d) Discoloured and brecciated karst surface atop biostrome three in section (e) Petrographic image (XPL) of an iron-stained fissure fill of detrital quartz grains from the Bunkers Sandstone (white arrow) in a dolomitised sample from (c). (f) Brecciated texture of a biostromal packstone, stained with Alizarin red S, calcite is red and dolomite does not stain. Secondary calcite veins (white arrow) crosscut the micritic matrix (PPL). Stained samples in (a), (b) and (f) are from Clarke (1988) samples JDAC 3-5-342, 3-5-353A, and, 3-5-379 respectively.	22
Figure 5: Sequence stratigraphic succession of the Wilkawillina Platform and adjacent basin.	25
Figure 6: Map of the Wilkawillina Platform	26
Figure 7: A physical stratigraphic model for the Wilkawillina platform and adjacent slope and basin (Bunkers graben) using two stratigraphic sections. SB = Sequence Boundary, MFS = Maximum Flooding Surface.	28
Figure 8: The covariance of $\delta^{13}\text{C}$ and $\delta^{18}\text{O}$ for section 1 (left) and section 2 (right). R^2 values do not show any significant linear relationship between $\delta^{13}\text{C}$ and $\delta^{18}\text{O}$	30
Figure 9: Stable isotope results for the Wilkawillina Platform correlated using the physical stratigraphic model.	31
Figure 10: Evolution of the $\delta^{13}\text{C}$ curve from the complete sections in Figure 9 to sequence packages as shown in Figure 11.	37
Figure 11: Chronostratigraphic diagram for the Wilkawillina Platform and adjacent basin. With $\delta^{13}\text{C}$ curve from sections 1 and 2	38
Figure 12: Conceptual chronostratigraphic diagram of the Maloof <i>et al.</i> (2010a) global composite $\delta^{13}\text{C}$ data. Based on chemostratigraphic sections from Maloof <i>et al.</i> (2005)	39

INTRODUCTION

The evolutionary appearance of complex life is widely believed to have been influenced by changing environmental conditions in Earth's biosphere (Hayes & Waldbauer 2006, Canfield *et al.* 2007, Maloof *et al.* 2010a). Environmental conditions, such as the concentration of free oxygen, thought to be key (Canfield *et al.* 2007), were a function of the carbon cycle (Killops & Killops 2009, Maloof *et al.* 2010a). The carbon cycle mediates the concentration of oxygen in the atmosphere and oceans through the amount of organic carbon compounds preserved in sedimentary rocks (Killops & Killops 2009). Early photosynthesising organisms fundamentally changed the Earth's exogenic cycle and hence, the carbon cycle through mediation of CO₂ and O₂ in the atmosphere and oceans (Derry *et al.* 1992, Hayes & Waldbauer 2006). The changes of the carbon cycle through time can be monitored using the ratio of the carbon 12 (¹²C) to the carbon 13 (¹³C) isotope in ancient sediments. This is because photosynthesis preferentially fractionates ¹²C from the dissolved carbon reservoir in seawater, leaving an enrichment of ¹³C. The ratio of ¹²C to ¹³C that is biologically mediated by primary productivity is known as δ¹³C measured against the reference standard PDB (Pee Dee Belemnite) in its units, per mille (‰). Intervals with positive δ¹³C relative to today's oceanic value of 0‰ are often considered to record enhanced organic carbon productivity in the oceans. However, it more accurately records the ratio of burial of organic carbon to inorganic carbon (carbonate). If carbonate deposition is constant through time, then an increase in δ¹³C indicates a greater fraction of organic carbon entering sediments. This ratio is most commonly measured in carbonate sediments that are thought to record marine depositional environments and thus the isotopic composition records the δ¹³C of seawater. The δ¹³C record shows variability

over geologic time, with some of the strongest variations coinciding with the intervals housing the Cambrian Explosion of Life. There is a possibility that this highly variable $\delta^{13}\text{C}$ record is representative of the Early Cambrian carbon composition of global seawater as $\delta^{13}\text{C}$ is predominantly precipitated with carbonates from the ocean. Therefore, the variability of $\delta^{13}\text{C}$ could be evidence of the reorganisation of carbon cycling that led to environmental changes conducive to evolution (Hayes & Waldbauer 2006, Maloof *et al.* 2010a). However, due to the carbon isotope mass balance and oxidant budgets of the Earth's oceans, there are some doubts about whether or not the changes in the $\delta^{13}\text{C}$ record are actually representative of the seawater values or other mechanisms (Swart & Eberli 2005, Bristow & Kennedy 2008, Swart 2008, Knauth & Kennedy 2009, Derry 2010, Swart & Kennedy 2012).

Previous authors have used the $\delta^{13}\text{C}$ record of ancient strata as a record of palaeo-environmental conditions, assuming that $\delta^{13}\text{C}$ records the global marine seawater signal of an isotopically well-mixed and thus isotopically homogeneous ocean (Brasier *et al.* 1990, Magaritz *et al.* 1991, Derry *et al.* 1994, Ripperdan 1994, Knoll *et al.* 1995a, Knoll *et al.* 1995b, Halverson *et al.* 2005, Maloof *et al.* 2005, Fike *et al.* 2006, Zhu *et al.* 2006, Kouchinsky *et al.* 2007, Maloof *et al.* 2010a, Fan *et al.* 2011, Grotzinger *et al.* 2011, Li *et al.* 2013). This interpretation was drawn from the reproducibility of similar $\delta^{13}\text{C}$ patterns within approximately synchronous stratigraphic profiles from carbonate platforms across the globe. Also, the assumption that precipitation of a shared $\delta^{13}\text{C}$ seawater value is the only mechanism responsible for the shared $\delta^{13}\text{C}$ pattern. The mean $\delta^{13}\text{C}$ value of the modern ocean is near 0‰ (Broecker & Peng 1982) however, in the ancient record, $\delta^{13}\text{C}$ shows extreme values that can vary from +10‰ to -12‰, which is

assumed to still be a primary marine signal by many authors (Hoffman *et al.* 1998, Fike *et al.* 2006, Zhu *et al.* 2006, Maloof *et al.* 2010a, Maloof *et al.* 2010b, Grotzinger *et al.* 2011). This is particularly evident at the Precambrian-Cambrian boundary, where fluctuations in the $\delta^{13}\text{C}$ record can shift 13‰ over only tens of meters of section.

Zhu *et al.* (2006) proposed a global composite $\delta^{13}\text{C}$ curve compiling data from studies in Siberia, China, USA, and Argentina. Maloof *et al.* (2010a) expanded on this global $\delta^{13}\text{C}$ curve compiling past and more recent $\delta^{13}\text{C}$ data from Siberia, Morocco, China, and Mongolia focussing on the Precambrian-Cambrian boundary. Their data shows several negative and positive excursions leading into the Cambrian with the most extreme shift being 13‰ over 3 million years. The composite $\delta^{13}\text{C}$ curves show several positive and negative excursions that could represent a fluctuating carbon cycle undergoing changes due to new influences, such as bioturbation, present in sediments after the appearance of the major metazoan groups (Hayes & Waldbauer 2006, Maloof *et al.* 2010a). The secular changes shown by Zhu *et al.* (2006), and Maloof *et al.* (2010a) have been correlated across the studied carbonate platforms, and are assumed to be reproducible. However, few of these sections have independent time constraints provided by biostratigraphy, radiometric dating, or a coeval deep-ocean record. Due to this, sections rely heavily on correlation using $\delta^{13}\text{C}$ data (chemostratigraphy). These authors have proposed the first hypothesis of this study; that $\delta^{13}\text{C}$ values are representative of marine values because secular variation implies all carbonates precipitating have a shared marine source.

Large magnitude $\delta^{13}\text{C}$ shifts in seawater like those posed for the Neoproterozoic and Early Cambrian occur in the Phanerozoic, but are inconsistent with the current

understanding of oxidant budgets, bulk mantle $\delta^{13}\text{C}$ values, and carbon cycling (Swart & Eberli 2005, Bristow & Kennedy 2008, Swart 2008, Derry 2010, Swart & Kennedy 2012). The carbon isotope mass balance is the balance of the $\delta^{13}\text{C}$ for organic and inorganic carbon in the ocean, written mathematically as:

$$\delta^{13}\text{C}_{tc} = (1 - X_{org})\delta^{13}\text{C}_{carb} + (X_{org})(\delta^{13}\text{C}_{org})$$

Where, $\delta^{13}\text{C}_{tc}$ is the total exogenic carbon (TC) assumed to equal the bulk Earth $\delta^{13}\text{C}$ value ($\delta^{13}\text{C}_{tc} = -5.5\text{‰}$), $\delta^{13}\text{C}_{carb}$ is the average $\delta^{13}\text{C}$ value of the sedimentary carbonate reservoir, and $\delta^{13}\text{C}_{org}$ is the average $\delta^{13}\text{C}$ value of the sedimentary organic carbon reservoir. X_{org} is the fraction of carbon in the reservoir that is organic ($X_{org} = M_{org}/M_{tc}$), where M_{org} and M_{tc} are the masses of organic and TC, respectively (Kump 1991, Derry *et al.* 1992). From this equation it has been shown that $\delta^{13}\text{C}$ values at the Precambrian-Cambrian boundary demand large amounts of oxidation, violate the carbon isotope mass balance (Bristow & Kennedy 2008).

If all photosynthetic life was removed from the ocean, the resultant ‘‘Strangelove’’ ocean (Broecker & Peng 1982, Hsü & McKenzie 1985) would have a $\delta^{13}\text{C}$ value of $\sim -6\text{‰}$, the canonical mantle value (Kump & Arthur 1999). This is the same lower limit for $\delta^{13}\text{C}$ due to enhanced volcanic activity (Renne *et al.* 1995). Other mechanisms that can cause negative shifts in the $\delta^{13}\text{C}$ record stem from the rapid injection of pools of depleted carbon which include; methane clathrate release, ocean stagnation and overturn, and oxidative decay of exposed marine organic sediments (Bristow & Kennedy 2008). These inputs sum up to $\delta^{13}\text{C}$ values of -5‰ over >200 thousand years (Bristow & Kennedy 2008). However, many excursions in the Precambrian and Cambrian have values much lighter than this (up to -12‰) that persist over longer time frames (millions of years) and are assumed to represent the global steady state open-marine value, and

therefore a large perturbation in the carbon cycle (Halverson *et al.* 2005, Maloof *et al.* 2005, Fike *et al.* 2006, Zhu *et al.* 2006, Maloof *et al.* 2010a, Maloof *et al.* 2010b).

Alternative mechanisms can account for these extreme $\delta^{13}\text{C}$ values. These include environmental variability, the influence of physiological fractionation by different organisms living on carbonate platforms, and diagenetic alteration. Carbonate platforms are a selective repository of ancient carbonate sediments, as deeper water sediments deposited on oceanic crust predating the Jurassic period (~180 Ma) have been removed from the sedimentary record by subduction. There are a few exceptions, such as; intracratonic basins that were once ancient seas connected to the open-ocean, or oceanic sediments preserved on continental crust through faulting or folding. Therefore, the ancient $\delta^{13}\text{C}$ record is comprised predominantly from carbonate sediments precipitated on platforms, not the open marine environment that provides marine values through the Cenozoic. Carbonate platforms form proximal to land where local processes can override marine influences. Swart and Eberli (2005) show the effect that shallow water, platformal environments proximal to landmasses have on $\delta^{13}\text{C}$ values. The smaller water volume found on carbonate platforms can lead to stratification and lateral variability. These factors can alter the $\delta^{13}\text{C}$ value of the smaller carbon reservoir quite easily. This leads to the $\delta^{13}\text{C}$ values having more extreme values than the isotopically well-mixed open marine system.

Carbonate platforms formed wholly or partly by photosynthetic organisms can have their $\delta^{13}\text{C}$ signal altered by physiologically controlled fractionation of carbon isotopes known as vital effects. Changes in $\delta^{13}\text{C}$ within an organism can occur due to the mixing of marine and metabolic CO_2 (Erez 1978).

Diagenesis is another important factor to consider when studying shallow carbonate sediments. Carbonate sediments are highly susceptible to diagenetic alteration, experiencing eogenesis (shallow, low temperature diagenesis) within the first few centimetres of burial (Ulmer-Scholle 2003). The effect of diagenesis must be considered when analysing the $\delta^{13}\text{C}$ values of carbonate sediments as it can be pervasive in and shift $\delta^{13}\text{C}$ values to very different values to those of coeval marine water. Exposure during sea level fall can lead to pervasive alteration to negative $\delta^{13}\text{C}$ values that assumes a systematic shape like a seawater excursion when sea level rises again and carbonate deposition is renewed. Diagenesis may also cause little-to-no alteration to the $\delta^{13}\text{C}$ if the fluid is sourced from local host rock, as the extent of alteration is dependent on the origin of the fluid, the isotopic mixing of different fluids, and host rock (Derry 2010). However, diagenetic alteration commonly gives rise to extremely negative $\delta^{13}\text{C}$ values derived from ^{12}C rich organic acids dissolved in meteoric waters (Swart & Eberli 2005, Swart 2008, Swart & Kennedy 2012).

Hence, the influence of depositional environment, vital effects on platforms, and diagenetic alteration are all important factors to consider when studying the $\delta^{13}\text{C}$ of carbonate sediments, as any alteration will change the $\delta^{13}\text{C}$ values from a marine origin. This leads to the second hypothesis; the $\delta^{13}\text{C}$ values of carbonate sediments do not correlate to marine $\delta^{13}\text{C}$ values (or between sections) because of local effects on carbon isotope composition. These effects are a) platformal variability and b) diagenesis.

The central piece of evidence for the marine origin of $\delta^{13}\text{C}$ hypothesis is that stratigraphic variations in the $\delta^{13}\text{C}$ values represent secular change in seawater and are thus reproducible in similar aged sections globally. This reproducibility of $\delta^{13}\text{C}$ is used

to correlate sections within the same study area or between separate basins. However, this method doesn't take into account the lithological relationships within sections or across basins. Therefore, the facies relationships are not represented accurately, leading to inaccurate interpretation of the stratigraphy and apparent deposition of shelf facies at the same time as deep water facies.

Sequence stratigraphy is 'the subdivision of sedimentary basin fills into genetic packages bounded by unconformities and their correlative conformities' (Emery & Myers 1996). The sequence stratigraphic approach can model the relationship of sedimentary facies in a chronostratigraphic framework. This model can show breaks in deposition and change in depositional mode previously unknown from individual stratigraphic sections or chemostratigraphy. Sequence boundaries (SB) are time surfaces represented by unconformities, where everything above is younger than everything below. There can be no correlation of lithologies that lay either side of that boundary; correlation can only occur with sections deposited at the same time interval (Figure 1; Emery and Myers (1996)). Using these SB, accurate correlation between sections is possible, leading to the accurate representation of the $\delta^{13}\text{C}$ record in ancient sections. When the $\delta^{13}\text{C}$ values of non-marine facies are removed this can lead to the conclusion that the marine $\delta^{13}\text{C}$ record of the past is fragmented and represents only a fraction of the time in which deposition is occurring. This leads to third and final hypothesis; the $\delta^{13}\text{C}$ values of carbonate sediments do not correlate to the marine $\delta^{13}\text{C}$ values (or between sections) because the stratigraphic record is incomplete.

The Wilkawillina Platform in the Central Flinders Ranges is arguably one of the best preserved Early Cambrian carbonate platforms in the geologic record. The carbon

isotope record of this succession has yet to be established, so it presents a unique opportunity to study such a well preserved carbonate platform for $\delta^{13}\text{C}$. The study area encompasses a complete section from platform through to the slope and basin providing an ideal framework to test the sequence stratigraphic approach. Evidence of SB run through the area as karst or exposure surfaces usually found between carbonate and siliciclastic units. Diagenetic alteration in the area is not pervasive, so some primary marine $\delta^{13}\text{C}$ values may be preserved. The Wilkawillina Platform provides a rare opportunity to test competing hypotheses regarding the $\delta^{13}\text{C}$ record and the depositional environments by enabling a sequence stratigraphic approach.

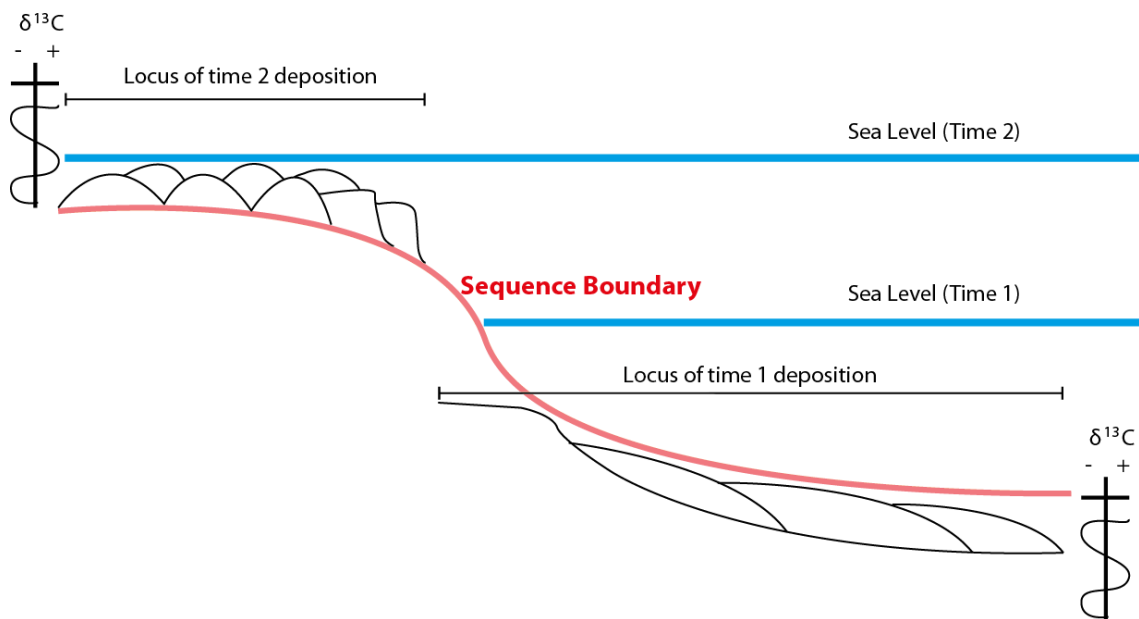


Figure 1: Sequence boundaries separate lithologies, facies, and stable isotope signals; even if previously correlated. Only the younger stratigraphy lying above the SB can be correlated, and the older stratigraphy below, but never the stratigraphy from either side of the SB. Hence only $\delta^{13}\text{C}$ values from the same side of the boundary can be correlated.

GEOLOGICAL SETTING

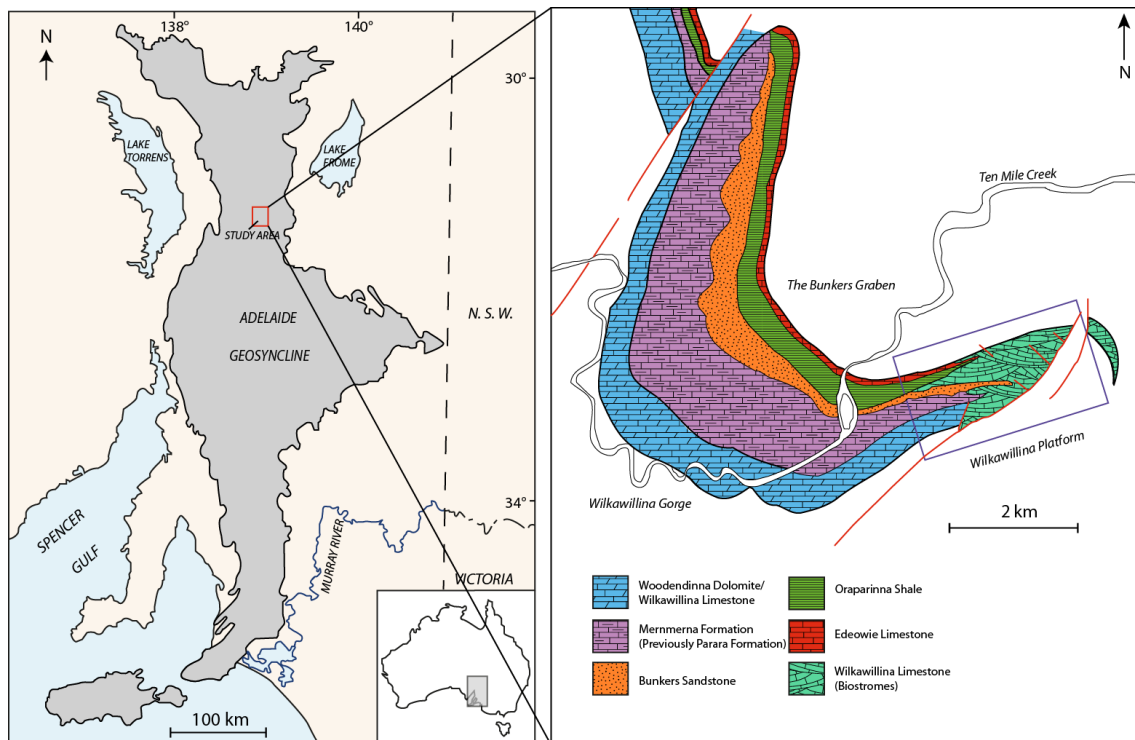


Figure 2: Location Map for the Wilkawillina Platform, Flinders Ranges, South Australia.

The Wilkawillina Platform is situated in the Central Flinders Ranges, in South Australia (Figure 2). The platform, as described by Clarke (1990), is an Early Cambrian (Atdabanian to Botoman; Jago et al. (2006)) carbonate platform which contains three large biostromes rich in Archaeocyatha and calcified microbial microfossils (calcimicrobes; Clarke (1990), James and Gravestock (1990)). The Siberian division of the Early Cambrian is used in this study, after Gravestock (1995), and Jago *et al.* (2002). This area is well known for its excellent preservation and has interested geologists and biostratigraphers alike. The platform lies on the south-eastern margin of the Bunkers Graben in the Arrowie Basin. The graben was folded during the Delamerian Orogeny and exposed during uplift in the Tertiary so the graben and adjacent platform can be easily studied in outcrop (Dalgarno 1964, Gravestock 1995).

This provides a rare exposure of an almost complete shelf to basin depositional environment.

The Wilkawillina platform isn't the only area where Archaeocyathan rich biostromes or bioherms are found in the Flinders Ranges. They are found as isolated 1m to 3m mounds of Wilkawillina Limestone throughout the Flinders Ranges where the Early Cambrian Hawker group is preserved (James & Gravestock 1990, Kruse 1991, Lafuste *et al.* 1991, Fuller & Jenkins 2007). No other Archaeocyathan build ups are found to be on the same scale as found on the Wilkawillina Platform.

The Early Cambrian Hawker Group (Dalgarno 1964) in this study area unconformably overlies the lower Pound Quartzite. This is a result of uplift and erosion of the Ediacaran member of the Pound Quartzite towards the end of the Proterozoic (Walter 1967), and also the erosion of the earliest unit of the Hawker Group, the Parachilna Formation (Dalgarno 1964). The Hawker group is conformably overlain by the younger Billy Creek Formation (Dalgarno 1964).

Deposition of the Hawker group was strongly controlled by the interaction of tectonics and relative sea level within the Arrowie basin. Subsidence rates along the south-eastern margin of the Bunkers Graben were significantly lower during the Early Cambrian than in the rest of the graben. This resulted in the persistence of shallow water conditions on the edge of an inland sea, enabling the formation of a carbonate platform at low latitudes (5°N of the equator; Clarke (1990), Gravestock (1995)). This platform was also subjected to periods of low sea level which caused sub-aerial exposure of the platform, cessation of carbonate deposition and the subsequent formation of exposure and karst surfaces (Clarke 1990). The major bounding fault of the graben was active

during the Early Cambrian. Evidence of this syn-sedimentary faulting include; wedges of conglomerates of the underlying Pound group, microfaulting of the Mernmerna formation, and changes in the thickness of stratigraphic units (Clarke 1990). The movement of the fault caused a thinning of the Bunkers Sandstone as the depositional environment changed due to uplift on the basin margin (platform) following a thickening of the underlying Wilkawillina Limestone as the platform sediments were deposited. The faulting in the area is related to the salt tectonics in the Oraparinna Diapir (Dalgarno 1964, Clarke 1990).

Thin tuff beds up to 2m thick indicate volcanism in the study area. These beds have been related to fault re-activation along the Torrens Hinge Zone as a result of the first tectonic phase of the Kangarooian Movements (Daily & Forbes 1969). This also caused uplift of the Willyama Inliers to the East followed by widespread erosion in the Arrowie basin prior to the deposition of the late Edeowie Limestone (Gravestock 1995); a possible source of the siliciclastic units (Bunkers Sandstone and Oraparinna Shale). The tuff beds, which are characteristically bottle green, outcrop a few metres below the uppermost exposure of the Wilkawillina Limestone and have only been given an imprecise U-Pb zircon age of 564 ± 61 Ma by Fanning (1987) (Gravestock 1995). Other geochronology in the Arrowie basin has been published by Gravestock and Shergold (2001), and Jenkins *et al.* (2002), but may not be reliable due to a conflict with biostratigraphic ages (522.0 ± 2.1 Ma; Jenkins *et al.* (2002) and 522.0 ± 1.8 Ma; Gravestock and Shergold (2001), (Hall *et al.* 2012)).

Following the Cambrian, the Adelaide Geosyncline experienced the Early and Middle Palaeozoic Delamerian Orogeny. Although the orogeny was highly deformational in other areas of the Adelaide Geosyncline; the Arrowie basin in the Central Flinders Ranges experienced only minor burial metamorphism and no igneous activity. However, folding, reactivation of major faults, and diapirism during the Ordovician Delamerian events was experienced within this region. Following this, there was some Cenozoic fault reactivation that has been recorded by fault breccias caused by some late-stage diapiric intrusions (Gravestock 1995).

METHODS

Field work was undertaken on the Wilkawillina Platform on the south-eastern margin of the Bunkers Graben. Stratigraphic sections based on the previous field study of Clarke (1988) were measured for stable isotope analysis. A 2km by 1km map of the area was drawn using an aerial photo tile from the Department for Manufacturing, Innovation, Trade, Resources and Energy (DMITRE, provided by Bob Dalgarno). Stratigraphic sections were measured using a Jacob Staff (Compton 1985) and 650 samples were taken for stable isotope and petrographic analysis along the two 1km stratigraphic section transects.

Stable isotope ($\delta^{18}\text{O}$ and $\delta^{13}\text{C}$) measurements were performed on 104 samples of ~0.8 mg powders, drilled from a fresh surface, using continuous-flow isotope-ratio mass spectrometry (CF-IRMS). Measurements were made on an Analytical Precision AP2003 at University of Melbourne. Results were normalised to the Vienna Pee Dee Belemnite scale (VPDB; modern equivalent of PDB) using internal working standards of Carrara Marble (NEW1 – Newcastle). Accepted mean analytical precision based on the repeat analyses of standards for $\delta^{18}\text{O}$ and $\delta^{13}\text{C}$ was 0.07‰ and 0.03‰ respectively for the first batch, 0.09‰ ($\delta^{18}\text{O}$) and 0.04‰ ($\delta^{13}\text{C}$) for the second batch, and 0.04 (for both $\delta^{18}\text{O}$ and $\delta^{13}\text{C}$) for the third batch (R. Drysdale, 2013, pers. comm.).

Twelve Petrographic samples were prepared at the University of Adelaide's lapidary and 38 thin sections from the study of Clarke (1988) were kindly loaned from the School of Environment at Flinders University. Detailed methods can be found in Appendix A.

OBSERVATIONS AND RESULTS

Stratigraphic Sections

Two 1Km sections were measured on the Wilkawillina platform and adjacent slope to basin recorded as stratigraphic section logs in Figure 3. The sections show a progression from shallow water deposition of the Woodendinna Dolomite recrystallised shelf facies of oolite shoals (Figure 4a) to deeper water deposition in the basin (Oraparinna Shale), while biostromes of Archaeocyatha developed on the shelf. The two sections are separated by approximately 1 km.

Section 1 contains six lithological units representing a transition from shelf to basin facies, capped by a return to shallow water deposition with the Edeowie Limestone. The Wilkawillina Limestone is primarily preserved here as small build ups of Archaeocyatha and ooid shoals. The Bunkers Sandstone is highly weathered in poor outcrop forming an erosional low overlying a correlative exposure surface. This siliciclastic unit has been recrystallised with a carbonate to dolomitic cement pervasive enough to induce a reaction with HCl (Figure 4b). Two lithologies are present in this section that are absent in section 2; the Oraparinna Shale and the Edeowie Limestone. The Oraparinna Shale represents the second siliciclastic unit present in the section and shows a basin-ward shift in facies after a correlative exposure surface. The surface represents a fall in sea-level, and hence, a sequence boundary (SB). The Edeowie Limestone is composed of shallow water carbonate sediments preserved here as micro-laminated dolomitic limestone, thought to have been deposited after the basin filled in a peritidal environment that was often sub-aerially exposed (Clarke 1990).

Section 2 preserves the evolution of the carbonate platform from small isolated build ups of Archaeocyatha and ooid shoals to large biostromes and lagoonal

environments with exposure surfaces, recording at least four sea-level falls. The Wilkawillina Limestone is the dominant lithology in this section. The Bunkers Sandstone is seen as a thin (1-2m) transgressive recrystallised unit overlying an exposure surface between the platformal Wilkawillina Limestone and the first biostrome build up.

Sequence boundaries in the area are represented by exposure surfaces. Four have been observed in both sections and were mapped continuously between the sections. They are identifiable in outcrop by; erosive contact with the overlying unit, discoloration, brecciation, a basinal shift in facies, infilling of fissures by detrital material (grykes), and recrystallisation (Figure 4c, d). Petrographic samples show discoloration, brecciation, micro-scale grykes, recrystallisation, and meteoric cements (Figure 4b, e, f). The sequence boundaries are conformably overlain by siliciclastic units in the basin section (section 1) and biostromal packstone to floatstone in the platform section (section 2).

All of these observations are evidence for karst surfaces, that extend <10 m below the contact with the above bed. Erosion at these boundaries is made evident by the sharp contact with overlying units, but it is impossible to know how much carbonate sediment has been lost, and thus, how much of the history has been eroded.

The facies chart below details the key features of each marine facies found in the Wilkawillina Platform area.

Table 1: Facies Chart of the Wilkawillina Platform and adjacent basin.

Facies	Lithological Units	Features
Platform	Wilkawillina Limestone Edeowie Limestone	Biostromal packstones and floatstones, fossils of Archaeocyatha and algae (<i>Renalcis</i> , <i>Girvanella</i> and some <i>Epiphyton</i>). Evaporite pseudomorphs in the Edeowie Limestone. Exposure surfaces on the top of biostromes highlighted by discoloured dolomite.
Shelf	Wilkawillina Limestone Woodendinna Dolomite	Ooid shoals, stromatolites. Some detrital fragments of Archaeocyatha and platform strata. Woodendinna Dolomite composed of oolite subjected to meteoric and burial diagenesis
Slope	Mernmerna Formation Calcareous Oraparinna Shale	Small (cm) and large (2m) slumps, microfaulting and silty interbeds in the Mernmerna. Detrital grain flows from the platform to calcareous transgressive units of the Oraparinna. Sponge spicules, fragments of Archaeocyatha, Echinoderms, and Trilobites in both Oraparinna and Mernmerna units.
Basin	Bunkers Sandstone Oraparinna Shale	Siliciclastic units, sandstone and shales. Sandstone is medium to coarse grained, well sorted quartz rich and carbonate cemented. Shale is green fine grained silty unit that features detrital calcareous grainflows from the platform.

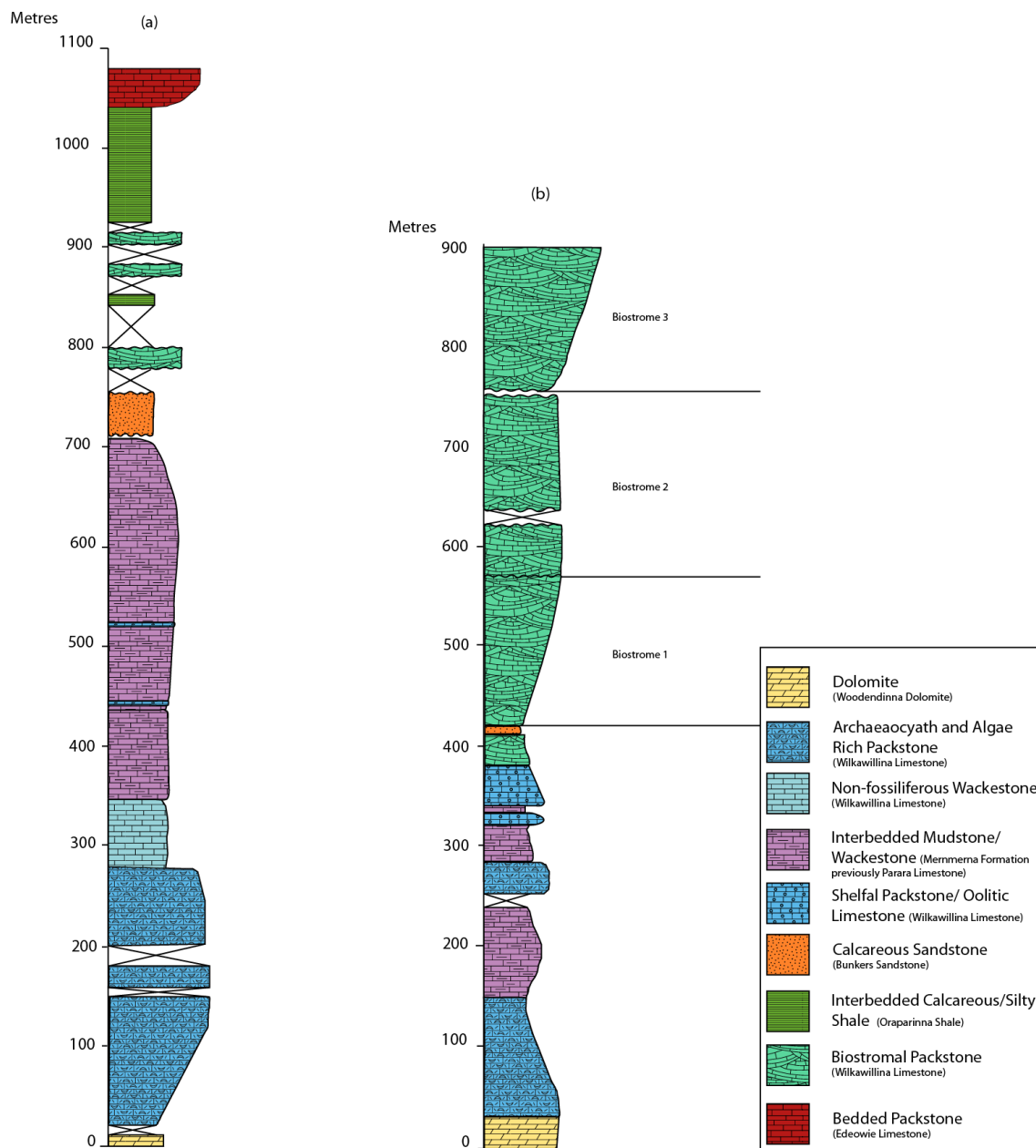


Figure 3: (a) Section 1 represents the slope to basin facies of the Wilkawillina platform. (b) Section 2 represents the slope to platformal facies.

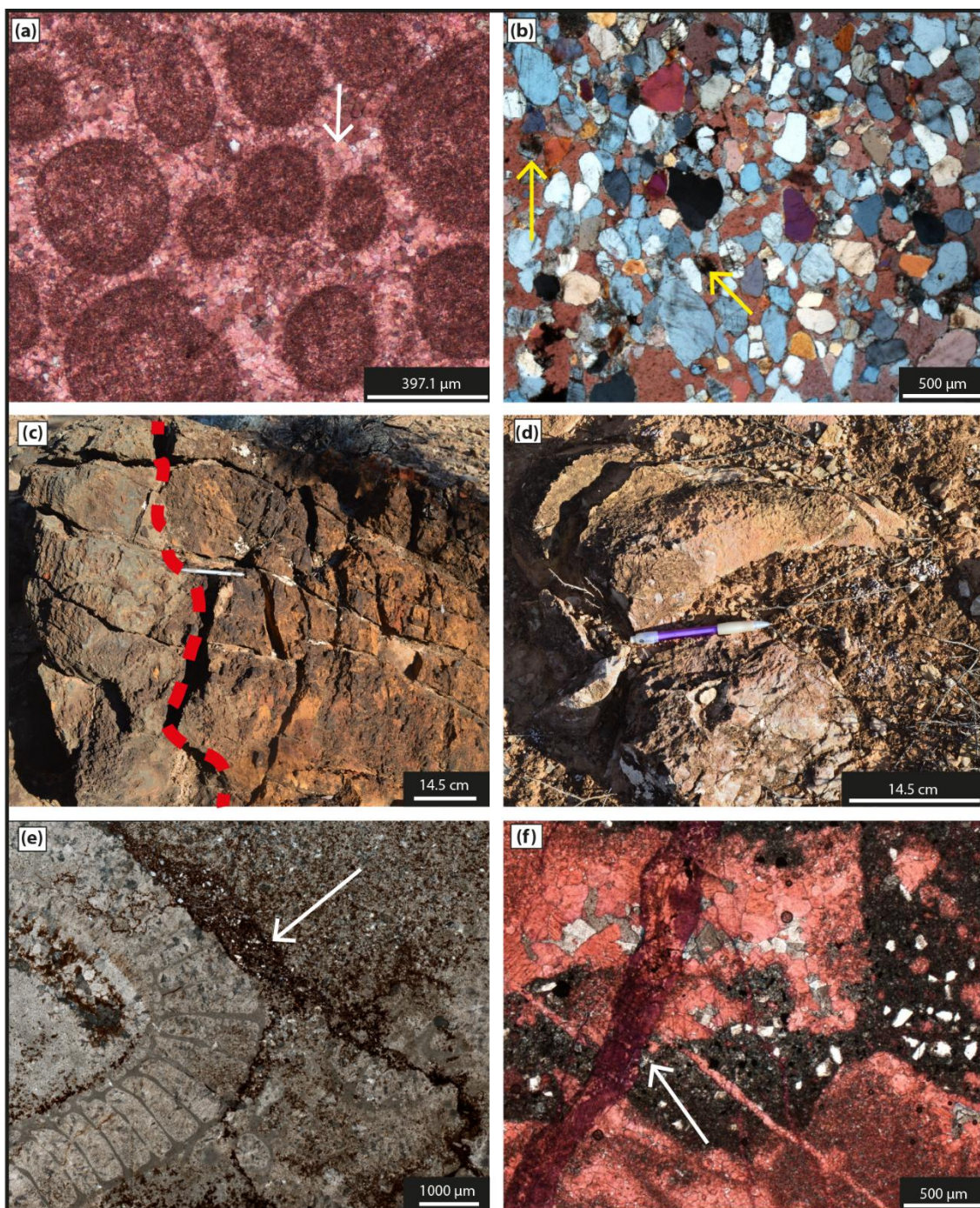
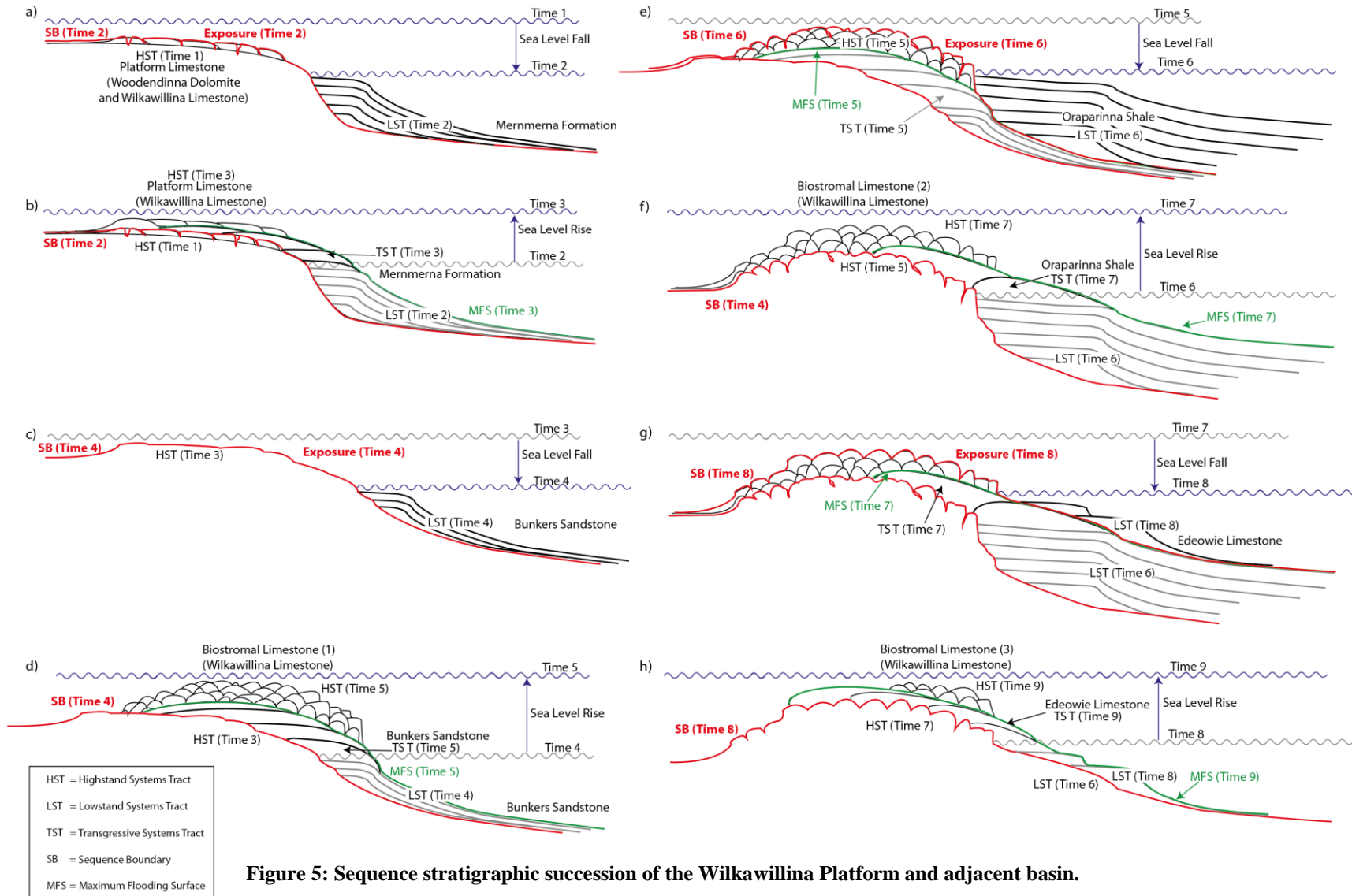


Figure 4: Evidence of diagenetic alteration. (a) Recrystallised oolite of the Woodendinna Dolomite stained with Alizarin red S, note the meteoric calcite cements infilling pore spaces around ooids (equant calcite; white arrow, XPL). **(b)** Recrystallised Bunkers Sandstone stained with Alizarin red S, calcite (red) and dolomite (yellow arrows) fill pore spaces in an interlocking pattern with quartz grains (XPL). **(c)** Red-dashed line shows the dolomitic front of discolouration at a karst surface. **(d)** Discoloured and brecciated karst surface atop biostrome three in section **(e)** Petrographic image (XPL) of an iron-stained fissure fill of detrital quartz grains from the Bunkers Sandstone (white arrow) in a dolomitised sample from **(c)**. **(f)** Brecciated texture of a biostromal packstone, stained with Alizarin red S, calcite is red and dolomite does not stain. Secondary calcite veins (white arrow) crosscut the micritic matrix (PPL). Stained samples in **(a)**, **(b)** and **(f)** are from Clarke (1988) samples JDAC 3-5-342, 3-5-353A, and, 3-5-379 respectively.

Sequence Stratigraphy

Figure 5 shows the detailed sequence stratigraphic succession of the Wilkawillina Platform and adjacent basin. The first lowstand is represented by the Mernmerna Formation overlying the SB on top of the shelfal Woodendinna Dolomite and Wilkawillina Limestone in section 1. Transgression is shown by the slope facies of the Mernmerna in section 2. Highstand is represented by the Wilkawillina Limestone platformal facies of ooid shoals and small build ups of Archaeocyatha. Sea-level fall is represented by the second exposure surface at the top of the oolitic facies of the Wilkawillina platform in section 2. The second lowstand is represented by the Bunkers Sandstone which overlies the SB on top of the oolitic Wilkawillina Limestone in section 1, the sandstone unit onlaps onto the slope in section 2 from the basin (section 1) in the east. This is immediately followed by a transgressive system tract (TST) composed of more Bunkers Sandstone onlapping to the platform, depositing as a shelf facies and infilling karstic fissures. Successive beds back-step up to the platform during progressive sea-level rise and a landward shift of the shoreline occurs. This causes beds to pinch out, as shown on the map in Figure 6. This is followed by highstand, in which deposition of carbonate sediments on the platform builds basinward as biostromal carbonates of the Wilkawillina Limestone. This cycle occurs a third time at the SB above biostrome 1, where the Oraparinna Shale is deposited at lowstand and during the transgressive phase. The cycle is followed by a highstand of platform packstone and floatstone from biostrome 2 in section 1 and 2. The final sequence shows the Edeowie limestone being deposited at lowstand and transgression in a shallow marine setting due to the low accommodation space present in the basin at the time of deposition. The formation is present in section 1 and pinches out on the map just before the platform

section. Carbonate deposition is again resumed on the platform as biostromal packstone and floatstone (biostrome 3).



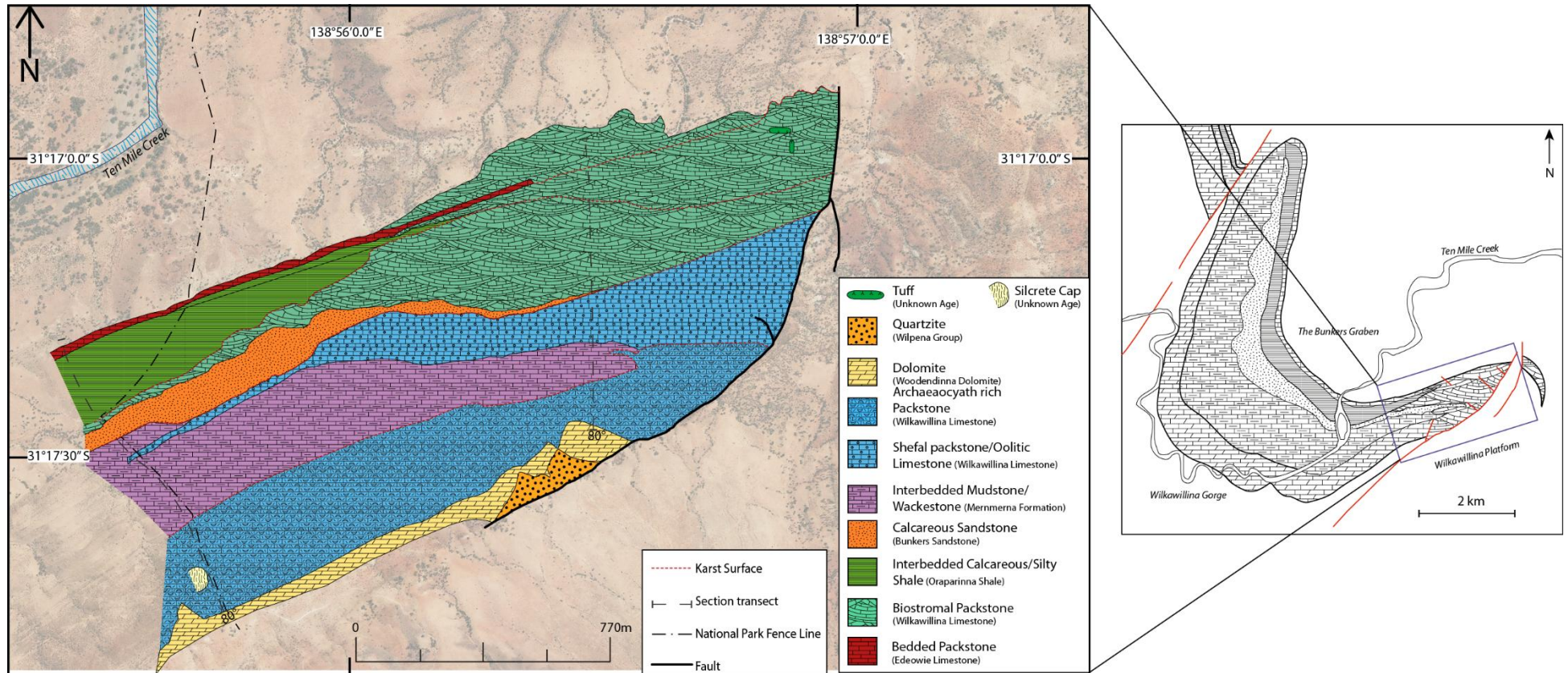


Figure 6: Map of the Wilkawillina Platform

Physical stratigraphic model

The stratigraphic model shown in Figure 7 has been based on the sequence stratigraphy of the Wilkawillina platform (Figure 5). Field observations of facies and surfaces within the mapping area coupled with petrographic analysis enabled the construction of the sequence stratigraphy and subsequently, this physical stratigraphic model.

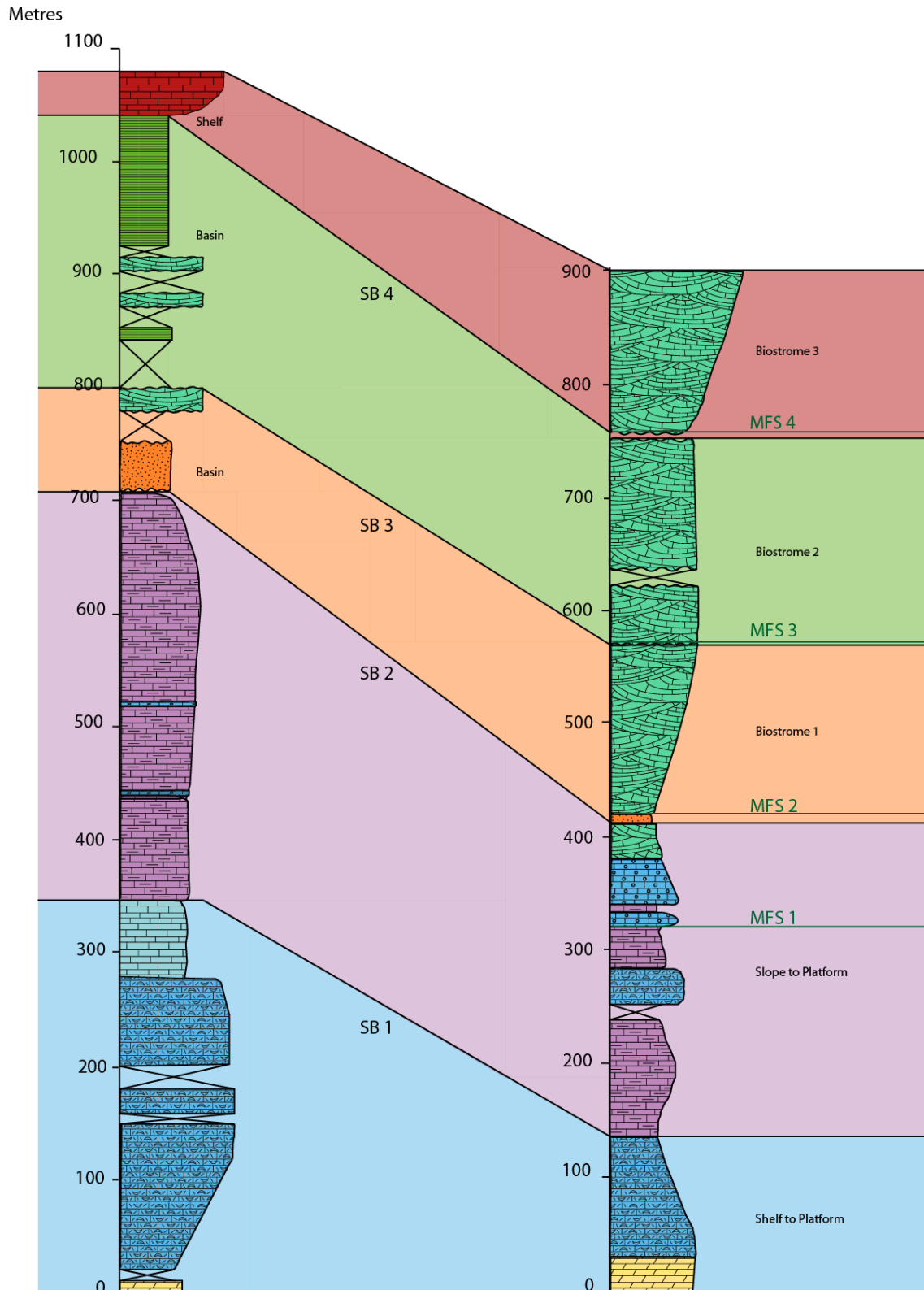


Figure 7: A physical stratigraphic model for the Wilkawillina platform and adjacent slope and basin (Bunkers graben) using two stratigraphic sections. SB = Sequence Boundary, MFS = Maximum Flooding Surface.

Stable Isotopes

After the two sections were correlated using the exposure surfaces (recall these surfaces represent SB) and physical stratigraphic model (Figure 7), the $\delta^{13}\text{C}$ values could be accurately compared. Figure 8 showed no significant covarying relationship between $\delta^{13}\text{C}$ and $\delta^{18}\text{O}$ for either section, however, there are a few exceptions to this as described below.

Section 1 (slope to basin) has a generally negative $\delta^{13}\text{C}$ trend with a lowest value of -3.05‰, the most positive value is +1.86‰. The negative trend indicates a slight depletion in the $\delta^{13}\text{C}$ source. Negative $\delta^{13}\text{C}$ values of the Bunkers Sandstone (-4.14‰ and -3.42‰) are very low and have undergone pervasive weathering and recrystallisation of the unit that may have influenced the $\delta^{13}\text{C}$ values (Figure 4b).

Changes in $\delta^{13}\text{C}$ values in Section 2 (platform) are out of phase with the slope/basin section as they show a positive $\delta^{13}\text{C}$ trend with most values plotting around 0‰ to +1‰. The most extreme values are -5.75‰ in the recrystallised dolomite, or -2.46‰ and +2.03‰ in unaltered limestones. The $\delta^{13}\text{C}$ values of this section are representative of $\delta^{13}\text{C}$ values from the isotopically well-mixed zone of the modern ocean.

The physical stratigraphy model shows that the platform and the basin/slope cannot be correlated based solely on the synchronicity of $\delta^{13}\text{C}$ values (Figure 9). Correlation has been achieved through time significant sequence boundaries which reveal $\delta^{13}\text{C}$ values are not synchronous.

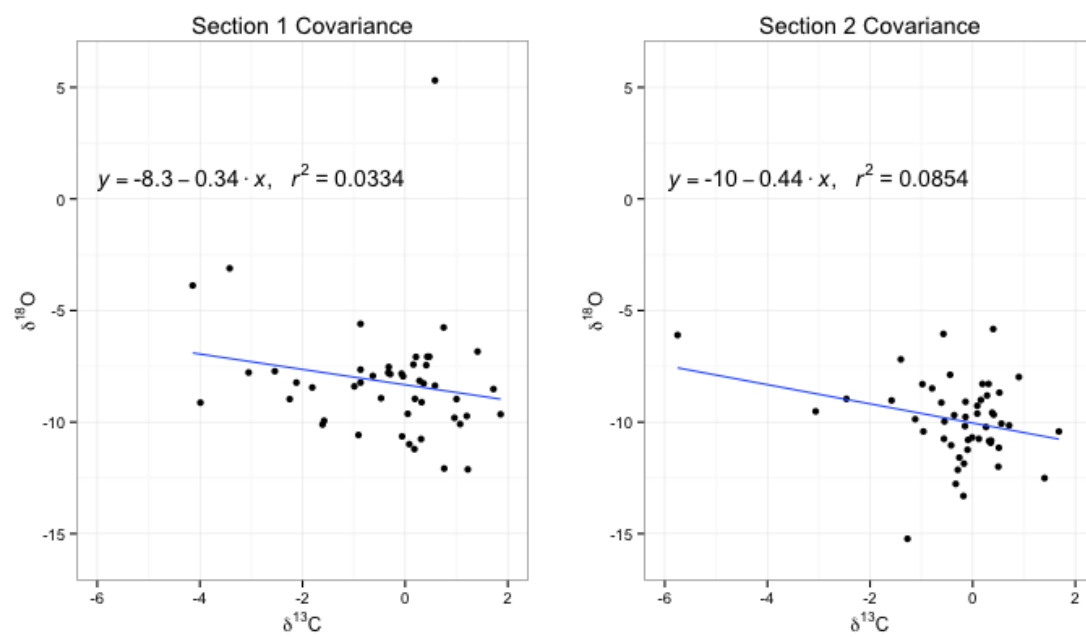


Figure 8: The covariance of $\delta^{13}\text{C}$ and $\delta^{18}\text{O}$ for section 1 (left) and section 2 (right). R^2 values do not show any significant linear relationship between $\delta^{13}\text{C}$ and $\delta^{18}\text{O}$.

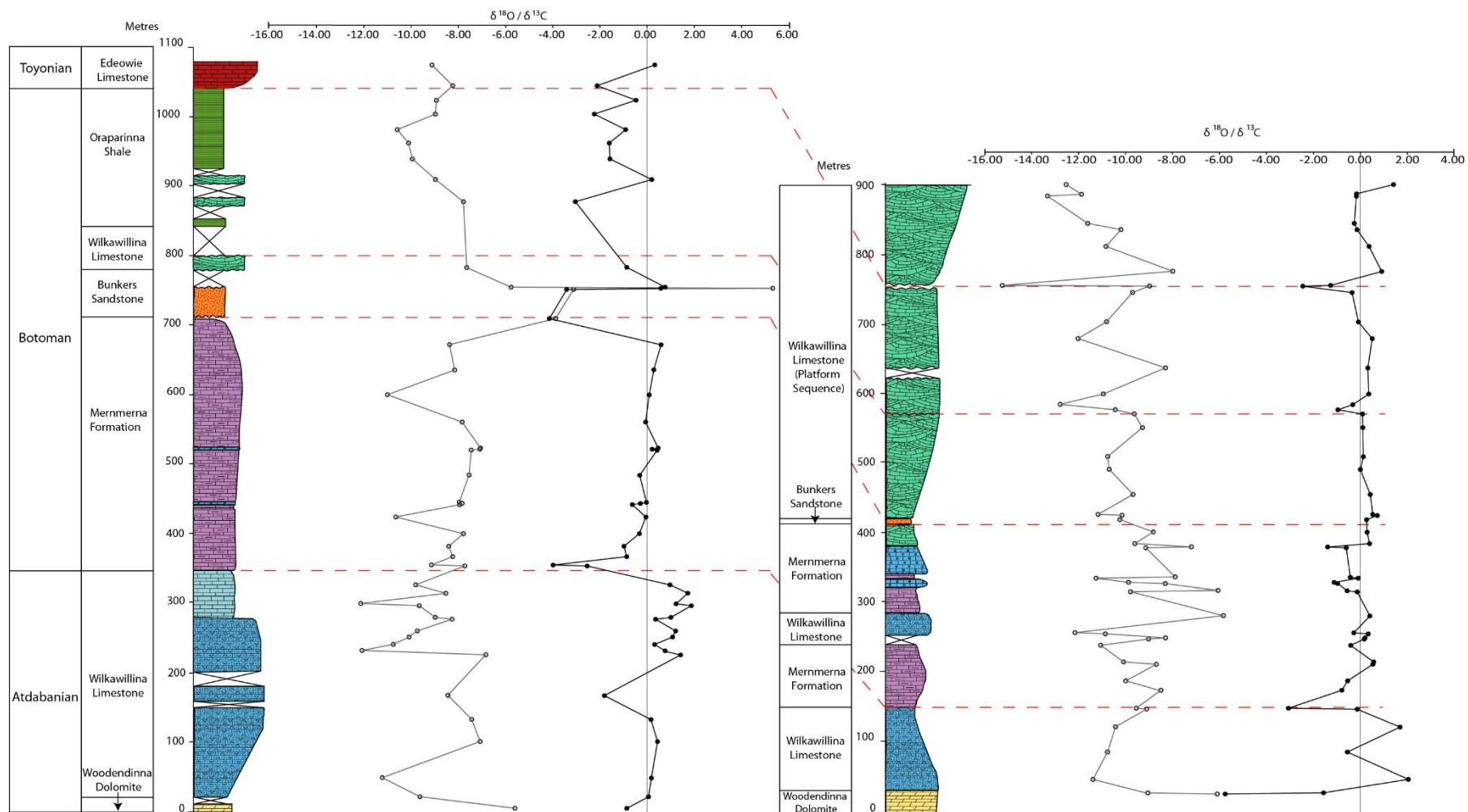


Figure 9: Stable isotope results for the Wilkawillina Platform correlated using the physical stratigraphic model.

DISCUSSION

Sequence stratigraphy can provide time significant information that is independent of chemostratigraphic correlation, and so provides a test of the time significance of the isotope values. Sequence stratigraphy uses the evidence of time surfaces, known as sequence boundaries (SB), to define packages of genetically related depositional cycles or sequences of lithologies and lithofacies. Sequence stratigraphy is useful in establishing the time relationships between different lithologies coinciding with different but synchronous depositional environments. Here, this approach has been used in the Wilkawillina Platform and adjacent basin to test the reproducibility of the $\delta^{13}\text{C}$ record over a short distance between sections with detailed time surfaces established in the field.

The ability to determine the duration or continuity of carbonate deposition through time in any given section is important for determining how much of the $\delta^{13}\text{C}$ record could have potentially been preserved. Only if carbonate deposition is continuous through time in a given location, can the $\delta^{13}\text{C}$ record be continuous. Sequence stratigraphy explicitly identifies areas of deposition and areas of non-deposition as the shoreline progrades and retreats in a basin. Chemostratigraphic studies assume that deposition of carbonate is continuous through time by presenting a complete $\delta^{13}\text{C}$ curve that shows no breaks.

The current notion of chemostratigraphy is that matching of shifts in $\delta^{13}\text{C}$ can serve as a basis for correlation (Derry et al. 1994, Halverson et al. 2005, Zhu et al. 2006, Maloof et al. 2010a, Bjerrum & Canfield 2011). The basis of chemostratigraphy is that

secular variation in the $\delta^{13}\text{C}$ of seawater causes a constant $\delta^{13}\text{C}$ value across platform and basin; therefore $\delta^{13}\text{C}$ values of the same time period are reproducible. The assumptions made by chemostratigraphic studies are; that carbonate platforms preserve all of the time they have been precipitating, carbonate platforms are representative of open marine environments, and alteration of $\delta^{13}\text{C}$ is low to not present, except where stated. From these studies, several conclusions have been drawn that relate to the palaeo-environmental conditions of Cambrian Explosion of Life and the carbon cycle of the early Phanerozoic. Maloof *et al.* (2010a) compiled a composite curve of $\delta^{13}\text{C}$ that shows a highly fluctuating curve during the Early Cambrian. The most extreme $\delta^{13}\text{C}$ shift of 13‰ from +7 to -6‰ is at the boundary of the Nemakit-Daldynian and Tommotian. After this large excursion, the $\delta^{13}\text{C}$ curve appears to settle with smaller magnitude shifts ranging from 8‰ down to 2‰. This is hypothesised to represent a stabilising carbon cycle as it begins to be mediated by life (Maloof *et al.* 2010a). However, the sections in this study have been correlated using only the reproducibility of the $\delta^{13}\text{C}$ curves of roughly the same age across two continents. Detailed sequence stratigraphy has not been applied to this study or other chemostratigraphic studies, so the duration and location of carbonate deposition has not been determined to evaluate how much time could potentially be recorded. This raises the question of whether the $\delta^{13}\text{C}$ values from these studies can be accurately placed stratigraphically or in geologic time.

Another complicating factor for chemostratigraphy is local variability due to vital effects or diagenesis. The $\delta^{13}\text{C}$ value of Archaeocyatha from the Wilkawillina Platform was found to be $-0.17\text{‰} \pm 0.04\text{‰}$, which is close to average modern seawater

values. However, there is still variation in $\delta^{13}\text{C}$ values between the platform and basin. This could be due to the proximal position of the platform to land or diagenesis.

The diagenetic effect on the platform is focused at the exposure surfaces, and in recrystallised sediments. Secondary cementation of the carbonate sediments and Bunkers Sandstone probably occurred during diagenesis when meteoric fluids passed through the sediment. Diagenetic influence is evident in the Bunkers Sandstone from recrystallisation infilling the pore spaces with equant calcite and dolomite (Figure 4b). These textures have negative $\delta^{13}\text{C}$ values in section 1 and co-variance with $\delta^{18}\text{O}$ (Figure 9); this negative shift and coupling of $\delta^{13}\text{C}$ and $\delta^{18}\text{O}$ is characteristic of meteoric diagenesis (Gross & Tracey 1966, Quinn 1991, Swart & Kennedy 2012). The Woodendinna Dolomite shows negative values between -0.87‰ and -5.75‰, equant and blocky calcite cements around ooids suggest a meteoric origin for the recrystallising fluid (Figure 4a). The diagenetic signature present at the karst surfaces has a characteristic negative $\delta^{13}\text{C}$ trend (between -0.96‰ and -4.14‰) and coupling of $\delta^{13}\text{C}$ and $\delta^{18}\text{O}$ that is again representative of meteoric alteration similar in trend to the Bunkers Sandstone alteration (Figure 9). The negative $\delta^{13}\text{C}$ values of meteoric diagenesis are caused by the introduction of ^{12}C rich fluids sourced from organic material in soil. When this meteoric fluid is mixed with more positive fluids from dissolved the carbonate sediments on the platform, it produces the negative trend observed in the $\delta^{13}\text{C}$ data (Gross & Tracey 1966, Quinn 1991, Marshall 1992).

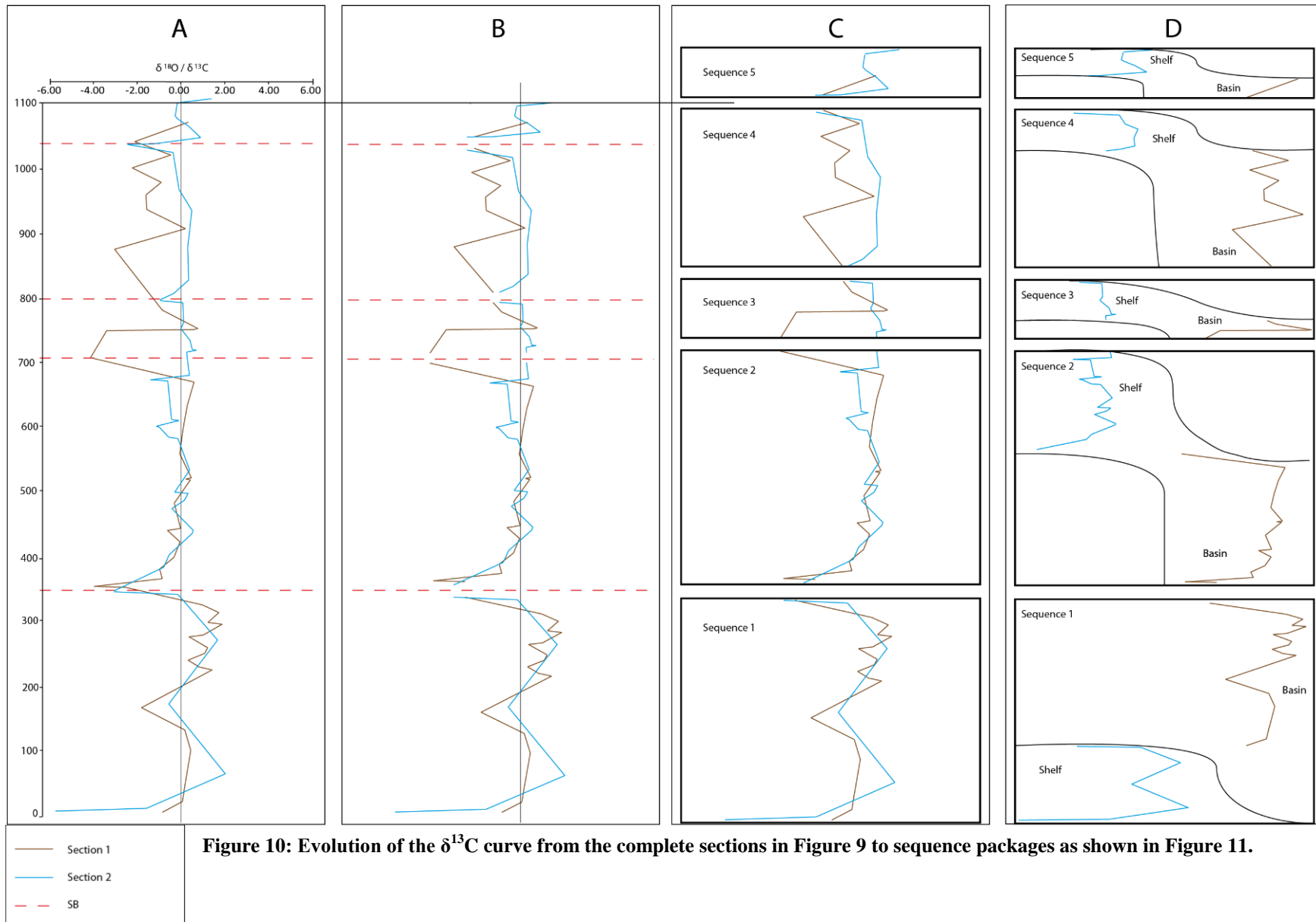
Chronostratigraphic diagrams can be applied to sedimentary basins to determine the amount of sediment preserved in different depositional environments through time. Figure 5 shows the sequence stratigraphic succession for the Wilkawillina Platform.

This model was converted into a chronostratigraphic diagram to determine how much depositional time was preserved. The presence of four SB shows that there were at least four breaks in carbonate deposition on the platform. From this, it is already clear that not all time was preserved on the platform, so carbonate sediments and therefore $\delta^{13}\text{C}$ data may be absent from the record. Figure 10 shows the evolution of the $\delta^{13}\text{C}$ curve from Figure 9 to the sequences in Figure 11.

Figure 11 shows the chronostratigraphic diagram incorporating sections 1 and 2 of the Wilkawillina platform and their $\delta^{13}\text{C}$ values. The diagram shows that there is not constant carbonate deposition on the carbonate platform over time. Carbonate deposition was interrupted by sea-level fall followed by a hiatus that lasted the extent of lowstand and transgression. When carbonate deposition resumed, it preserved a limited range of $\delta^{13}\text{C}$ values, which caused the development of an episodic curve. From the diagram in Figure 11 it is clear that constant carbonate deposition in one location in the basin, and continuous recording of the $\delta^{13}\text{C}$ curve is not possible with basic stratigraphic development in sedimentary basins.

Figure 12 shows a conceptual chronostratigraphic diagram for the Moroccan sections taken from the global $\delta^{13}\text{C}$ curve of Maloof *et al.* (2010a) and Maloof *et al.* (2005). In this conceptual diagram, carbonate deposition is shown to be continuous, as in the sections described in Maloof *et al.* (2005), and the $\delta^{13}\text{C}$ curve appears to be constant through time without breaks. The $\delta^{13}\text{C}$ values also correlate between basin and shelf facies. Figure 12 also shows the deposition of sedimentary packages in the basin at lowstand occurring at the same time as deposition occurs on the platform at highstand based on the chemostratigraphic correlation of Maloof *et al.* (2005). From a sequence stratigraphic point of view, this cannot happen. Therefore, the correlation of the isotope

curves must be incorrect and chemostratigraphy may be misinterpreting the origin and significance of $\delta^{13}\text{C}$ values.



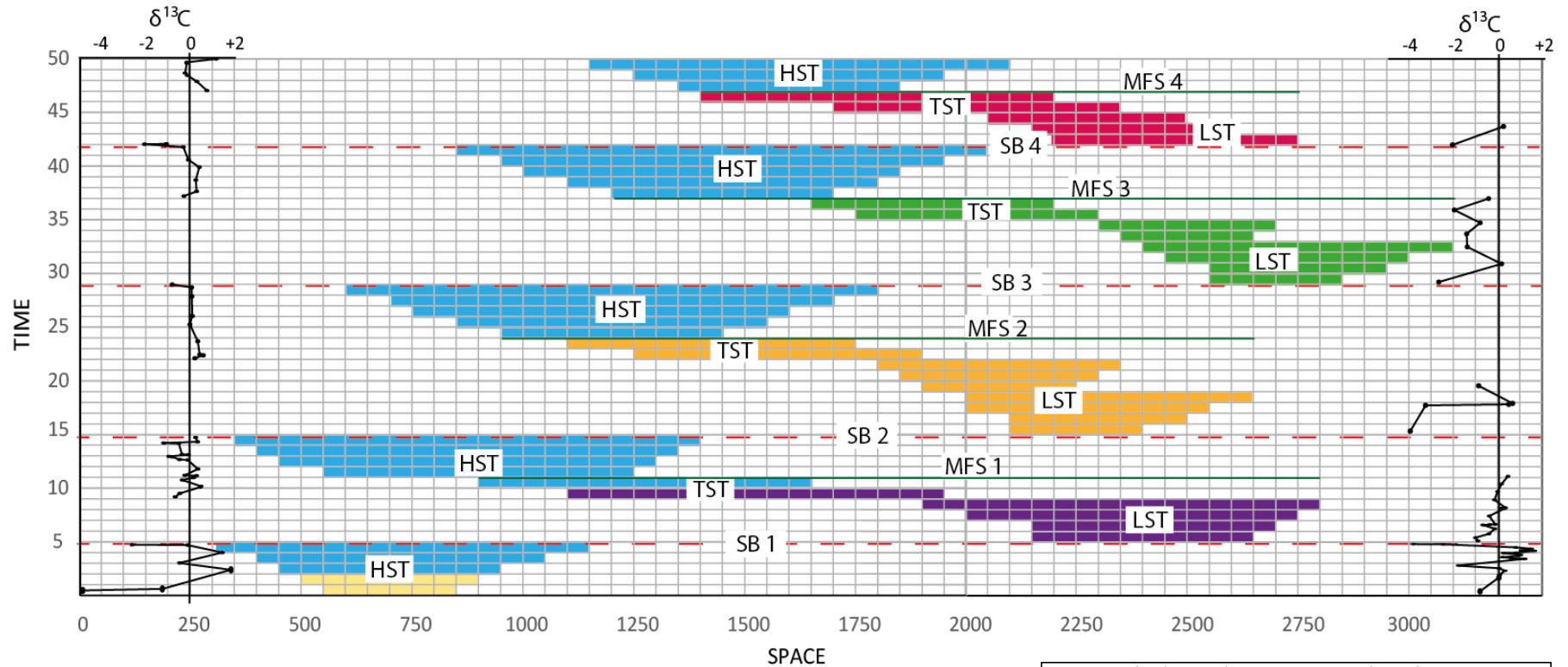








Figure 11: Chronostratigraphic diagram for the Wilkawillina Platform and adjacent basin. With $\delta^{13}C$ curve from sections 1 and 2

	Woodendinna Dolomite	HST = Highstand Systems Tract
	Wilkawillina Limestone	LST = Lowstand Systems Tract
	Mernmerna Formation	TST = Transgressive Systems Tract
	Bunkers Sandstone	SB = Sequence Boundary
	Oraparinna Shale	MFS = Maximum Flooding Surface
	Edeowie Limestone	

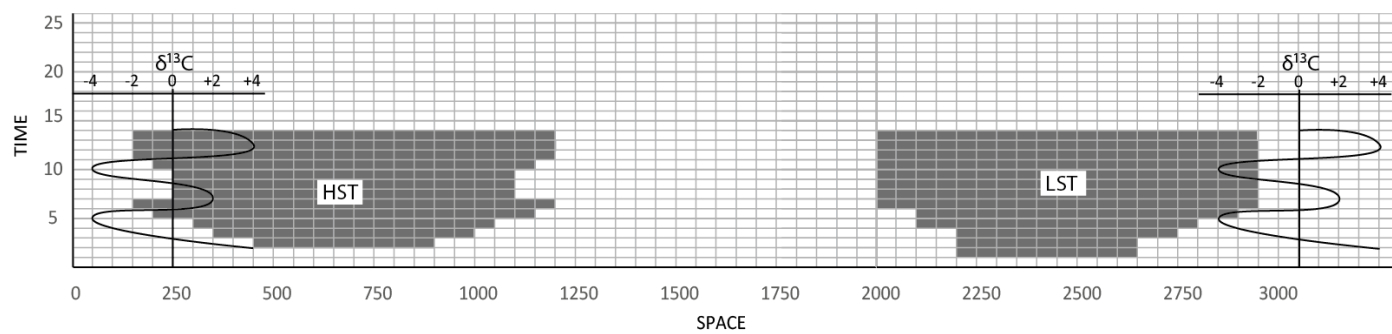


Figure 12: Conceptual chronostratigraphic diagram of the Maloof *et al.* (2010a) global composite $\delta^{13}\text{C}$ data. Based on chemostratigraphic sections from Maloof *et al.* (2005)

CONCLUSIONS

The $\delta^{13}\text{C}$ record of Early Cambrian is used as a proxy for the carbon cycle during a pivotal time in Earth history. The Cambrian Explosion of Life spans from the Precambrian-Cambrian boundary to the end of the Cambrian Period. Many authors have tried to document the changes in geology and geochemistry that lead to this diversification of life (Magaritz *et al.* 1986, Tucker 1989, Brasier *et al.* 1990, Kirschvink *et al.* 1991, Magaritz *et al.* 1991, Brasier *et al.* 1993, Kaufman *et al.* 1996, Zhu *et al.* 2001, Maloof *et al.* 2005, Ishikawa *et al.* 2008, Maloof *et al.* 2010a). These authors believe that reproducible excursions in $\delta^{13}\text{C}$ of correlated sections are representative of the carbon cycle at the Precambrian-Cambrian boundary. They hypothesise that the $\delta^{13}\text{C}$ record is precipitated from a marine source and represents shifts in the carbon cycle before the Cambrian Explosion. It is then hypothesised that the carbon cycle becomes mediated by new forms of life in the later stages of the Cambrian Explosion (Maloof *et al.* 2010a).

The interpretation of $\delta^{13}\text{C}$ leads to implications for a number of fields. If such a powerful proxy such as $\delta^{13}\text{C}$ does exist, it means that the palaeo-conditions of atmosphere and oceans that lead to the radiation of metazoans can be modelled. This model can then be applied in other fields such as palaeontology and astrobiology to determine the environmental conditions essential for the rapid evolution of life on a young habitable planet. However, this study shows through a sequence stratigraphic approach that carbonate deposition is not continuous through time and therefore, neither is the $\delta^{13}\text{C}$ record. Therefore, to preserve a marine $\delta^{13}\text{C}$, the slope to basin sediments of carbonate systems must be preserved in lowstand and transgressive stages, particularly

if the platform is affected by significant alteration. Hence, the origin of $\delta^{13}\text{C}$ must be carefully determined in order to properly interpret its significance and relevance to the carbon cycle.

Previous chemostratigraphic studies must be reviewed in light of this new approach. Several of the published studies on the Precambrian-Cambrian boundary and Cambrian explosion of Life use chemostratigraphy as a correlative tool (Brasier *et al.* 1994, Derry *et al.* 1994, Kouchinsky *et al.* 2001, Halverson *et al.* 2005, Maloof *et al.* 2005, Fike *et al.* 2006, Maloof *et al.* 2010a, Maloof *et al.* 2010b, Fan *et al.* 2011, Grotzinger *et al.* 2011). However, these studies should include a sequence stratigraphic framework to identify temporal continuation of the $\delta^{13}\text{C}$ record in order to interpret $\delta^{13}\text{C}$ as a proxy for the carbon cycle.

ACKNOWLEDGMENTS

First and foremost, I wish to thank my supervisor Martin Kennedy for teaching me how to become a professional geologist and researcher. I also thank Bob Dalgarno for his endless knowledge of the Flinders Ranges and for taking the time to assist me this year. I thank the PhD students Rob Klæbe and Alex Corrick for their help and patience this year. I thank Robyn Williamson for assisting me on my field work and carrying 650 samples of carbonate rocks back to camp. I also wish to thank Robyn and Troy Granger for being supportive Honours colleagues. I thank the fellow members of the Sprigg Geobiology Centre for their support and advice in the office and at lab meetings, particularly Tony Hall for assisting me with drafts. I wish to thank The Flinders Ranges National Park, Arthur Coulthard and The Farghers at Wirrealpa Station for allowing me to do fieldwork and collect samples on their land. I wish to thank Russell Drysdale and Warrick Joe at the University of Melbourne for allowing me the use of their AP2003 and for running the analysis on the stable isotope samples. I also thank Gail Jackson, Jonathon Clarke, the University of Adelaide, Adelaide Microscopy, ASP, Flinders University and DMITRE for providing materials and resources key to my project and thesis. Finally, I thank Katie Howard for being a great teaching support officer and helping out in times of need.

REFERENCES

- BJERRUM C. J. & CANFIELD D. E. 2011. Towards a quantitative understanding of the late Neoproterozoic carbon cycle. *Proceedings of the National Academy of Sciences* **108**, 5542-5547.
- BRASIER M., CORFIELD R., DERRY L., ROZANOV A. Y. & ZHURAVLEV A. Y. 1994. Multiple $\delta^{13}\text{C}$ excursions spanning the Cambrian explosion to the Botomian crisis in Siberia. *Geology* **22**, 455-458.
- BRASIER M., KHOMENOVSKY V. & CORFIELD R. 1993. Stable isotopic calibration of the earliest skeletal fossil assemblages in eastern Siberia (Precambrian-Cambrian boundary). *Terra Nova* **5**, 225-232.
- BRASIER M. D., MAGARITZ M., CORFIELD R., LUO H., WU X., OUYANG L., JIANG Z., HAMDI B., HE T. & FRASER A. 1990. The carbon-and oxygen-isotope record of the Precambrian-Cambrian boundary interval in China and Iran and their correlation. *Geological Magazine* **127**, 319-332.
- BRISTOW T. F. & KENNEDY M. J. 2008. Carbon isotope excursions and the oxidant budget of the Ediacaran atmosphere and ocean. *Geology* **36**, 863-866.
- BROECKER W. S. & PENG T.-H. 1982. *Tracers in the sea*. Lamont-Doherty Geological Observatory, Columbia University, Palisades, New York.
- CANFIELD D. E., POULTON S. W. & NARBONNE G. M. 2007. Late-Neoproterozoic deep-ocean oxygenation and the rise of animal life. *Science* **315**, 92-95.
- CLARKE J. 1988. Geology of the Hawker Group (Early Cambrian) at Wilkawillina Gorge, South Australia. PhD thesis, School of Earth Sciences, Flinders University (unpubl.).
- CLARKE J. 1990. An Early Cambrian carbonate platform near Wilkawillina Gorge, South Australia. *Australian Journal of Earth Sciences* **37**, 471-483.
- COMPTON R. R. 1985. *Geology in the Field*. John Wiley and Sons, New York, NY.
- DAILY B. & FORBES B. 1969. *Notes on the Proterozoic and Cambrian, southern and central Flinders Ranges, South Australia* (Geological excursions handbook, Vol. 22).
- DALGARNO C. 1964. Lower Cambrian stratigraphy of the Flinders Ranges. *Transactions of the Royal Society of South Australia* **88**, 129-144.
- DERRY L., BRASIER M., CORFIELD R. E. A., ROZANOV A. Y. & ZHURAVLEV A. Y. 1994. Sr and C isotopes in Lower Cambrian carbonates from the Siberian craton: A paleoenvironmental record during the 'Cambrian explosion'. *Earth and Planetary Science Letters* **128**, 671-681.
- DERRY L. A. 2010. A burial diagenesis origin for the Ediacaran Shuram–Wonoka carbon isotope anomaly. *Earth and Planetary Science Letters* **294**, 152-162.
- DERRY L. A., KAUFMAN A. J. & JACOBSEN S. B. 1992. Sedimentary cycling and environmental change in the Late Proterozoic: evidence from stable and radiogenic isotopes. *Geochimica et Cosmochimica Acta* **56**, 1317-1329.
- EMERY D. & MYERS K. 1996. *Sequence Stratigraphy*. Blackwell Science, Oxford.
- EREZ J. 1978. Vital effect on stable-isotope composition seen in foraminifera and coral skeletons. *Nature* **273**, 199-202.
- FAN R., DENG S. & ZHANG X. 2011. Significant carbon isotope excursions in the Cambrian and their implications for global correlations. *Science China Earth Sciences* **54**, 1686-1695.
- FANNING C. 1987. U-Pb zircon dating of a tuff interbedded with the Lower Cambrian Wilkawillina Limestone. *South Australian Department of Mines and Energy Open File Envelope (unpublished)*.
- FIKE D., GROTZINGER J., PRATT L. & SUMMONS R. 2006. Oxidation of the Ediacaran ocean. *Nature* **444**, 744-747.
- FULLER M. & JENKINS R. 2007. Reef corals from the Lower Cambrian of the Flinders Ranges, South Australia. *Palaeontology* **50**, 961-980.
- GRAVESTOCK D. 1995. Chapter 7: Early and Middle Palaeozoic. In: Drexel J. F. & Preiss W. V. eds., *The Geology of South Australia: The Phanerozoic*, Vol. 54, pp 3-61, Mines and Energy, South Australia, Geological Survey of South Australia.
- GRAVESTOCK D. I. & SHERGOLD J. H. 2001. Australian Early and Middle Cambrian sequence biostratigraphy with implications for species diversity and correlation. *The ecology of the Cambrian radiation*, 107-136.
- GROSS M. G. & TRACEY J. I. 1966. Oxygen and carbon isotopic composition of limestones and dolomites, Bikini and Eniwetok Atolls. *Science* **151**, 1082-1084.
- GROTZINGER J. P., FIKE D. A. & FISCHER W. W. 2011. Enigmatic origin of the largest-known carbon isotope excursion in Earth's history. *Nature Geoscience* **4**, 285-292.
- HALL P., HALVERSON G., COLLINS A., MCKIRDY D. & JAGO J. B. 2012. Filling the Australian Cambrian chemostratigraphic gap: Early Cambrian carbon isotopic profiles of three South Australian basins. PhD thesis, Earth and Environmental Sciences, University of Adelaide (unpubl.).

- HALVERSON G. P., HOFFMAN P. F., SCHRAG D. P., MALOOF A. C. & RICE A. H. N. 2005. Toward a Neoproterozoic composite carbon-isotope record. *Geological Society of America Bulletin* **117**, 1181-1207.
- HAYES J. M. & WALDBAUER J. R. 2006. The carbon cycle and associated redox processes through time. *Philosophical Transactions of the Royal Society B: Biological Sciences* **361**, 931-950.
- HOFFMAN P. F., KAUFMAN A. J., HALVERSON G. P. & SCHRAG D. P. 1998. A Neoproterozoic snowball earth. *Science* **281**, 1342-1346.
- HSÜ K. J. & MCKENZIE J. A. 1985. A "Strangelove" ocean in the earliest Tertiary. *Geophysical Monograph Series* **32**, 487-492.
- ISHIKAWA T., UENO Y., KOMIYA T., SAWAKI Y., HAN J., SHU D., LI Y., MARUYAMA S. & YOSHIDA N. 2008. Carbon isotope chemostratigraphy of a Precambrian/Cambrian boundary section in the Three Gorge area, South China: prominent global-scale isotope excursions just before the Cambrian Explosion. *Gondwana Research* **14**, 193-208.
- JAGO J., SUN X. & ZANG W. 2002. Correlation within early Palaeozoic basins of eastern South Australia. *Department of Primary Industry and Resources, South Australia, Report Book* **33**, 22.
- JAGO J., ZANG W.-L., SUN X., BROCK G., PATERSON J. & SKOVSTED C. 2006. A review of the Cambrian biostratigraphy of South Australia. *Palaeoworld* **15**, 406-423.
- JAMES N. P. & GRAVESTOCK D. I. 1990. Lower Cambrian shelf and shelf margin buildups, Flinders Ranges, South Australia. *Sedimentology* **37**, 455-480.
- JENKINS R., COOPER J. & COMPSTON W. 2002. Age and biostratigraphy of Early Cambrian tuffs from SE Australia and southern China. *Journal of the Geological Society* **159**, 645-658.
- KAUFMAN A. J., KNOLL A. H., SEMIKHATOV M. A., GROTZINGER J. P., JACOBSEN S. B. & ADAMS W. 1996. Integrated chronostratigraphy of Proterozoic-Cambrian boundary beds in the western Anabar region, northern Siberia. *GEOLOGICAL MAGAZINE-LONDON* **133**, 509-533.
- KILLOPS S. D. & KILLOPS V. J. 2009. *Introduction to organic geochemistry*. Wiley. com.
- KIRSCHVINK J. L., MAGARITZ M., RIPPERDAN R. L., ZHURAVLEV A. Y. & ROZANOV A. Y. 1991. The Precambrian-Cambrian boundary: magnetostratigraphy and carbon isotopes resolve correlation problems between Siberia, Morocco, and South China. *GSA Today* **1**, 69-91.
- KNAUTH L. P. & KENNEDY M. J. 2009. The late Precambrian greening of the Earth. *Nature* **460**, 728-732.
- KNOLL A. H., GROTZINGER J. P., KAUFMAN A. J. & KOLOSOV P. 1995a. Integrated approaches to terminal Proterozoic stratigraphy: an example from the Olenek Uplift, northeastern Siberia. *Precambrian Research* **73**, 251-270.
- KNOLL A. H., KAUFMAN A. J., SEMIKHATOV M. A., GROTZINGER J. P. & ADAMS W. 1995b. Sizing up the sub-Tommotian unconformity in Siberia. *Geology* **23**, 1139-1143.
- KOUCHINSKY A., BENGTSON S., MISSARZHEVSKY V. V., PELECHATY S., TORSSANDER P. & VAL'KOV A. K. 2001. Carbon isotope stratigraphy and the problem of a pre-Tommotian Stage in Siberia. *Geological Magazine* **138**, 387-396.
- KOUCHINSKY A., BENGTSON S., PAVLOV V., RUNNEGAR B., TORSSANDER P., YOUNG E. & ZIEGLER K. 2007. Carbon isotope stratigraphy of the Precambrian-Cambrian Sukharikha River section, northwestern Siberian platform. *Geological Magazine* **144**, 609.
- KRUSE P. D. 1991. Cyanobacterial-archaeocyathan-radiocyathan bioherms in the Wirrealpa Limestone of South Australia. *Canadian Journal of Earth Sciences* **28**, 601-615.
- KUMP L. R. 1991. Interpreting carbon-isotope excursions: Strangelove oceans. *Geology* **19**, 299-302.
- KUMP L. R. & ARTHUR M. A. 1999. Interpreting carbon-isotope excursions: carbonates and organic matter. *Chemical Geology* **161**, 181-198.
- LAFUSTE J., DEBRENNE F., GANDIN A. & GRAVESTOCK D. 1991. The oldest tabulate coral and the associated archaeocyatha, Lower Cambrian, Flinders Ranges, South Australia. *Geobios* **24**, 697-718.
- LI D., LING H.-F., SHIELDS-ZHOU G. A., CHEN X., CREMONESE L., OCH L., THIRLWALL M. & MANNING C. J. 2013. Carbon and strontium isotope evolution of seawater across the Ediacaran–Cambrian transition: Evidence from the Xiaotan section, NE Yunnan, South China. *Precambrian Research* **225**, 128-147.
- MAGARITZ M., HOLSER W. T. & KIRSCHVINK J. L. 1986. Carbon-isotope events across the Precambrian/Cambrian boundary on the Siberian Platform.
- MAGARITZ M., KIRSCHVINK J. L., LATHAM A. J., ZHURAVLEV A. Y. & ROZANOV A. Y. 1991. Precambrian/Cambrian boundary problem: Carbon isotope correlations for Vendian and Tommotian time between Siberia and Morocco. *Geology* **19**, 847-850.
- MALOOF A. C., PORTER S. M., MOORE J. L., DUDÁS F. Ö., BOWRING S. A., HIGGINS J. A., FIKE D. A. & EDDY M. P. 2010a. The earliest Cambrian record of animals and ocean geochemical change. *Geological Society of America Bulletin* **122**, 1731-1774.

- MALOOF A. C., RAMEZANI J., BOWRING S. A., FIKE D. A., PORTER S. M. & MAZOUAD M. 2010b. Constraints on early Cambrian carbon cycling from the duration of the Nemakit-Daldynian–Tommotian boundary $\delta^{13}\text{C}$ shift, Morocco. *Geology* **38**, 623-626.
- MALOOF A. C., SCHRAG D. P., CROWLEY J. L. & BOWRING S. A. 2005. An expanded record of Early Cambrian carbon cycling from the Anti-Atlas Margin, Morocco. *Canadian Journal of Earth Sciences* **42**, 2195-2216.
- MARSHALL J. D. 1992. Climatic and oceanographic isotopic signals from the carbonate rock record and their preservation. *Geological Magazine* **129**, 143-160.
- QUINN T. M. 1991. Meteoric diagenesis of plio-pleistocene limestones at Enewetak atoll. *Journal of Sedimentary Research* **61**, 681-703.
- RENNE P. R., BLACK M. T., ZICHAO Z., RICHARDS M. A. & BASU A. R. 1995. Synchrony and causal relations between Permian-Triassic boundary crises and Siberian flood volcanism. *Science* **269**, 1413-1416.
- RIPPERDAN R. 1994. Global variations in carbon isotope composition during the latest Neoproterozoic and earliest Cambrian. *Annual Review of Earth and Planetary Sciences* **22**, 385-417.
- SWART P. & KENNEDY M. J. 2012. Does the global stratigraphic reproducibility of $\delta^{13}\text{C}$ in Neoproterozoic carbonates require a marine origin? A Pliocene–Pleistocene comparison. *Geology* **40**, 87-90.
- SWART P. K. 2008. Global synchronous changes in the carbon isotopic composition of carbonate sediments unrelated to changes in the global carbon cycle. *Proceedings of the National Academy of Sciences* **105**, 13741-13745.
- SWART P. K. & EBERLI G. 2005. The nature of the $\delta^{13}\text{C}$ of periplatform sediments: Implications for stratigraphy and the global carbon cycle. *Sedimentary Geology* **175**, 115-129.
- TUCKER M. E. 1989. Carbon isotopes and Precambrian—Cambrian boundary geology, South Australia: ocean basin formation, seawater chemistry and organic evolution. *Terra Nova* **1**, 573-582.
- ULMER-SCHOLLE D. S. 2003. *A color guide to the petrography of carbonate rocks: grains, textures, porosity, diagenesis* (Vol. 77). AAPG Online Bookstore.
- WALTER M. 1967. Archaeocyatha and the biostratigraphy of the lower Cambrian Hawker Group, South Australia. *Journal of the Geological Society of Australia* **14**, 139-152.
- ZHU M.-Y., BABCOCK L. E. & PENG S.-C. 2006. Advances in Cambrian stratigraphy and paleontology: integrating correlation techniques, paleobiology, taphonomy and paleoenvironmental reconstruction. *Palaeoworld* **15**, 217-222.
- ZHU M., LI G. & ZHANG J. 2001. New C isotope stratigraphy from southwest China: Implications for the placement of the Precambrian-Cambrian boundary on the Yangtze Platform and global correlations: Comment and Reply. *Geology* **29**, 871-872.

APPENDIX A: METHODS

Please see attached file

APPENDIX B: SUPPLEMENTARY RESULTS

Please see attached file

APPENDIX A: METHODS

Methods

Field work and Sampling

Stratigraphic sections were logged using the Jacob's Staff method after Compton (1985) and sampled for stable isotope, geochemical and petrographic analysis. Collection of samples occurred every 3 m through the section and every 1 m at contacts between lithological units. GPS points were recorded in the notebook for the start and end of each section and for important features within the sections or between them. Mapping was done in the 2 km x 1 km area between the two stratigraphic sections to trace lithological units and surfaces to identify the relationship between the platform and basin palaeoenvironments. An aerial photo tile from DMITRE of the area was used as an A3 base for the map.

Sample Preparation (Isotopic Analysis)

Samples were mainly chosen based on association with lithological contacts and textures corresponding to diagenesis and unique lithologies (eg. Ooids, karsts). The remainder of the samples were chosen to represent a "skeleton" of the section using even spacing and a preference for limestones over dolomites. After selection, samples were washed and scrubbed to remove any dirt, lichen or mould that would contaminate the drilling. The samples were then drilled using a diamond tipped micro-drill for ~ 5 mg of powder. These were placed in small vials and labelled with the sample number. A total of 104 samples were drilled and analysed. Four samples were drilled for 200mg of powder for pressure calcimetry.

Pressure Calcimetry

Method adapted from Sherrod et al. (2002)

Normalized to the standards and blanks run in sync with the test to a polynomial equation trendline.

Step 1: Cut micro-centrifuge tubes just above the 1.0ml mark.

Step 2: Add 5 ml 4 M HCl/3% FeCl₂ solution to each glass vial.

Step 3: Weigh out 200mg of each sample into a cut micro-centrifuge tube and place this into a glass vial containing HCl acid. Make sure that the sample does not come into contact with the acid.

Step 4: Weigh out 7 CaCO₃ standards and place into vials containing acid. CaCO₃ standard weights: 200mg, 150mg, 100mg, 75mg, 50mg, 25mg and 10mg

Step 5: Cap all vials with a rubber stopper and a foil cap, and then crimp the foil using the hand crimper.

Step 6: Once all samples and standards to be tested are capped shake each vial vigorously to ensure that all of the samples reacts with the acid.

Step 7: Leave the vials sitting for half an hour, shaking them once more at the 15 min mark

Step 8: Attach the hose and needle to the manometer

Step 9: Tear out the centre of the aluminium cap on the first vial, pierce the rubber cap with the needle and record the maximum pressure vial. Repeat for all vials.

Step 10: The weight and pressure of the standards and pressure recorded in each sample is then used to calculate the equivalent mass of CaCO₃ in each sample. This value

needs to be normalized to the exact mass of sample weighed into each centrifuge tube.

This is most easily done in excel.

Step 11: Convert %CaCO₃ in each sample into % IC

To make the 4M HCl/3% FeCl₂: to prepare acid reagent mix 330 ml of concentrated (37%; 36.46 M) HCl with about 500 ml of water in a 1 L volumetric flask. Add 30 g ferrous chloride and dilute to total volume of 1 L.

Isotopic Analysis

Stable isotope ($\delta^{18}\text{O}$ and $\delta^{13}\text{C}$) measurements were performed on the evolved CO₂ gas of $\sim 0.8 \pm$ mg powders using continuous-flow isotope-ratio mass spectrometry (IRMS).

Measurements were made on an Analytical Precision AP2003 at University of

Melbourne. Samples were digested in 105% phosphoric acid at 70°C, mass

spectrometric measurements were made on the evolved CO₂ gas (Drysdale *et al.* 2009).

Results were normalised to the Vienna Pee Dee Belemnite scale using internal working standards of Carrara Marble (NEW1 – Newcastle), which was cross-checked against the international standards NBS18 and NBS19. Accepted mean analytical precision based

on the repeat analyses of standards for $\delta^{18}\text{O}$ and $\delta^{13}\text{C}$ was 0.07‰ and 0.03‰

respectively for the first batch and 0.09% and 0.04% respectively for the second batch

(R. Drysdale, 2013, pers. comm.).

Thin Section Preparation

Sub-samples of each lithology were taken as well as sub-samples of diagenetic textures

for analysis by petrography. Two samples of the diagenetic textures were cut to a size of

24X46 mm using a small rock saw in house. The samples were then sent to Prograding

Rock Services Ltd. (2280 – 39th Ave, NE, Calgary, AB, Canada) to be made into thin sections. Twelve samples were made in house using the University of Adelaide's Lapidary with 25X75 mm slides.

APPENDIX B: SUPPLEMENTARY RESULTS

Stable Isotope Results

Table 1: Stable Isotope results for Section 1

Prefix	Date	Sample No.	Metre	Lithology	$\delta^{13}\text{C}$	$\delta^{18}\text{O}$
CK	22/04/2013	4	6	Woodendinna Dolomite	-0.87	-5.60
CK	22/04/2013	5	22.5	Wilkawillina Limestone	0.05	-9.63
CK	22/04/2013	11	49.5	Wilkawillina Limestone	0.18	-11.21
CK	23/04/2013	15	102	Wilkawillina Limestone	0.43	-7.07
CK	23/04/2013	25	133.5	Wilkawillina Limestone	0.16	-7.42
CK	23/04/2013	32	168	Wilkawillina Limestone	-1.81	-8.45
CK	23/04/2013	37	190.5	Wilkawillina Limestone	-8.41	-5.51
CK	23/04/2013	40	226.5	Wilkawillina Limestone	1.41	-6.84
CK	23/04/2013	42	232.5	Wilkawillina Limestone	0.76	-12.08
CK	23/04/2013	45	241.5	Wilkawillina Limestone	0.31	-10.76
CK	23/04/2013	51	252	Wilkawillina Limestone	1.07	-10.09
CK	23/04/2013	54	261	Wilkawillina Limestone	1.20	-9.73
CK	23/04/2013	60	277.5	Wilkawillina Limestone	0.36	-8.27
CK	23/04/2013	62	280.5	Wilkawillina Limestone	1	-8.97
CK	23/04/2013	68	297	Wilkawillina Limestone	1.86	-9.65
CK	23/04/2013	69	300	Wilkawillina Limestone	1.22	-12.12
CK	23/04/2013	74	315	Wilkawillina Limestone	1.72	-8.52
CK	24/04/2013	5	327	Wilkawillina Limestone	0.96	-9.81
CK	24/04/2013	16	354	Wilkawillina Limestone	-2.54	-7.72
CK	24/04/2013	17	355.5	Mernmerna Formation	-3.99	-9.13
CK	24/04/2013	23	367.5	Mernmerna Formation	-0.87	-8.23
CK	24/04/2013	28	382.5	Mernmerna Formation	-0.99	-8.4
CK	24/04/2013	34	400.5	Mernmerna Formation	-0.33	-7.79
CK	24/04/2013	42	424.5	Mernmerna Formation	-0.06	-10.64
CK	24/04/2013	49	442.5	Mernmerna Formation	-0.63	-7.93
CK	24/04/2013	50	444	Wilkawillina Limestone	-0.29	-7.85
CK	24/04/2013	51	445.5	Mernmerna Formation	-0.04	-7.95
CK	25/04/2013	9	484.5	Mernmerna Formation	-0.32	-7.53
CK	25/04/2013	28	520.5	Mernmerna Formation	0.41	-7.45
CK	25/04/2013	29	522	Wilkawillina Limestone	0.21	-7.08
CK	25/04/2013	30	523.5	Mernmerna Formation	0.47	-7.07
CK	26/04/2013	13	561	Mernmerna Formation	-0.07	-7.83
CK	26/04/2013	26	600	Mernmerna Formation	0.08	-10.99
CK	26/04/2013	38	636	Mernmerna Formation	0.28	-8.15

CK	26/04/2013	50	672	Mernmerna Formation	0.58	-8.37
CK	26/04/2013	67	709.5	Bunkers Sandstone	-4.14	-3.88
CK	26/04/2013	68	751.5	Bunkers Sandstone	-3.42	-3.11
CK	26/04/2013	69	753	Bunkers Sandstone	0.58	5.31
CK	26/04/2013	70	754.5	Bunkers Sandstone	0.75	-5.76
CK	26/04/2013	71	783	Wilkawillina Limestone	-10.76	0.00
CK	26/04/2013	81	877.5	Wilkawillina Limestone	-3.05	-7.78
CK	26/04/2013	84	909	Wilkawillina Limestone	0.19	-8.96
CK	26/04/2013	88	939	Oraparinna Shale	-1.58	-9.94
CK	26/04/2013	90	961.5	Oraparinna Shale	-1.61	-10.11
CK	26/04/2013	96	981	Oraparinna Shale	-0.91	-10.58
CK	26/04/2013	101	1003.5	Oraparinna Shale	-2.25	-8.97
CK	26/04/2013	102	1023	Oraparinna Shale	-0.47	-8.93
CK	26/04/2013	103	1044	Edeowie Limestone	-2.12	-8.23
CK	26/04/2013	107	1074	Edeowie Limestone	0.32	-9.11

Table 2: Stable isotope results for Section 2

Prefix	Date	Sample No.	Metre	Lithology	$\delta^{13}\text{C}$	$\delta^{18}\text{O}$
CK	27/04/2013	12	27	Woodendinna Dolomite	-5.75	-6.10
CK	27/04/2013	13	28.5	Wilkawillina Limestone	-1.58	-9.03
CK	27/04/2013	23	48	Wilkawillina Limestone	2.03	-11.37
CK	27/04/2013	36	87	Wilkawillina Limestone	-0.56	-10.75
CK	27/04/2013	48	123	Wilkawillina Limestone	1.68	-10.42
CK	27/04/2013	59	148.5	Wilkawillina Limestone	-0.14	-9.09
CK	27/04/2013	60	150	Mernmerna Formation	-3.06	-9.52
CK	28/04/2013	7	175.5	Mernmerna Formation	-0.79	-8.49
CK	28/04/2013	16	189	Mernmerna Formation	-0.55	-9.97
CK	28/04/2013	27	213	Mernmerna Formation	0.52	-8.68
CK	28/04/2013	28	216	Wilkawillina Limestone	0.56	-10.07
CK	28/04/2013	36	240	Wilkawillina Limestone	-0.42	-11.04
CK	28/04/2013	39	249	Wilkawillina Limestone	0.16	-9.01
CK	28/04/2013	40	250.5	Mernmerna Formation	0.19	-8.29
CK	28/04/2013	44	256.5	Mernmerna Formation	0.32	-10.85
CK	28/04/2013	45	258	Wilkawillina Limestone	-0.29	-12.14
CK	28/04/2013	56	282	Mernmerna Formation	0.40	-5.83
CK	28/04/2013	70	316.5	Mernmerna Formation	-0.14	-9.77
CK	28/04/2013	71	318	Wilkawillina Limestone	-0.57	-6.05
CK	28/04/2013	77	328.5	Wilkawillina Limestone	-0.98	-8.30
CK	28/04/2013	78	330	Mernmerna Formation	-1.12	-9.87
CK	28/04/2013	82	336	Mernmerna Formation	-0.10	-11.24

CK	28/04/2013	83	337.5	Wilkawillina Limestone	-0.44	-7.88
CK	28/04/2013	99	379.5	Wilkawillina Limestone	-0.61	-9.13
CK	28/04/2013	100	381	Wilkawillina Limestone	-1.40	-7.19
CK	28/04/2013	102	385.5	Wilkawillina Limestone	0.38	-9.58
CK	28/04/2013	109	402	Wilkawillina Limestone	0.28	-8.81
CK	28/04/2013	116	420	Bunkers Sandstone	0.26	-10.22
CK	28/04/2013	117	426	Bunkers Sandstone	0.71	-10.15
CK	28/04/2013	118	427.5	Wilkawillina Limestone	0.51	-11.15
CK	28/04/2013	128	456	Wilkawillina Limestone	0.41	-9.67
CK	28/04/2013	140	492	Wilkawillina Limestone	-0.01	-10.69
CK	28/04/2013	146	510	Wilkawillina Limestone	0.12	-10.75
CK	29/04/2013	10	552	Wilkawillina Limestone	0.09	-9.27
CK	29/04/2013	17	571.5	Wilkawillina Limestone	0.09	-9.62
CK	29/04/2013	21	577.5	Wilkawillina Limestone	-0.96	-10.42
CK	29/04/2013	25	585	Wilkawillina Limestone	-0.33	-12.77
CK	29/04/2013	30	600	Wilkawillina Limestone	0.35	-10.93
CK	29/04/2013	42	637.5	Wilkawillina Limestone	0.31	-8.29
CK	29/04/2013	56	679.5	Wilkawillina Limestone	0.5	-12
CK	29/04/2013	64	703.5	Wilkawillina Limestone	-0.09	-10.80
CK	29/04/2013	78	745.5	Wilkawillina Limestone	-0.36	-9.69
CK	29/04/2013	82	754.5	Wilkawillina Limestone	-2.46	-8.96
CK	29/04/2013	83	756	Wilkawillina Limestone	-1.27	-15.23
CK	29/04/2013	91	775.5	Wilkawillina Limestone	0.9	-7.98
CK	29/04/2013	103	811.5	Wilkawillina Limestone	0.36	-10.83
CK	29/04/2013	111	835.5	Wilkawillina Limestone	-0.15	-10.18
CK	29/04/2013	114	844.5	Wilkawillina Limestone	-0.26	-11.59
CK	29/04/2013	127	883.5	Wilkawillina Limestone	-0.18	-13.31
CK	29/04/2013	128	886.5	Wilkawillina Limestone	-0.17	-11.86
CK	29/04/2013	133	900	Wilkawillina Limestone	1.40	-12.51

Standard Errors

Table 3: Standard error for Batch 1

Name	C Corrected to VPDB	O Corrected to VPDB
NEW1	2.31	-2.54
NEW1	2.36	-2.37
NEW1	2.39	-2.42
NEW1	2.47	-2.33
NEW1	2.38	-2.55
NEW1	2.39	-2.46
NEW1	2.41	-2.33
NEW1	2.41	-2.65
NEW1	2.40	-2.45
NEW1	2.40	-2.47
NEW1	2.39	-2.58
NEW1	2.37	-2.40
NEW1	2.42	-2.23
NEW1	2.44	-2.40
NEW1	2.40	-2.41
NEW1	2.42	-2.50
NEW1	2.39	-2.58
NEW1	2.42	-2.53
NEW1	2.40	-2.53
NEW1	2.42	-2.47
NEW1	2.38	-2.49
NEW1	2.37	-2.37
NEW1	2.44	-2.53
NEW1	2.42	-2.46
NEW1	2.40	-2.51
NEW1	2.44	-2.46
NEW1	2.39	-2.52
NEW1	2.33	-2.58

NEW1	2.40	-2.42
NEW1	2.43	-2.43
NEW1	2.47	-2.50
NEW1	2.42	-2.48
NEW1	2.39	-2.32
NEW1	2.36	-2.38
NEW1	2.39	-2.33
NEW1	2.44	-2.34
NEW1	2.39	-2.47
NEW1	2.36	-2.49
NEW1	2.40	-2.61
NEW1	2.39	-2.50
NEW1	2.34	-2.52
NEW1	2.42	-2.51
NEW1	2.41	-2.45
NEW1	2.46	-2.26
NEW1	2.40	-2.41
NEW1	2.41	-2.44
NEW1	2.39	-2.33
NEW1	2.41	-2.42
NEW1	2.41	-2.49
NEW1	2.45	-2.29
NEW1	2.38	-2.54
NEW1	2.39	-2.46
NEW1	2.37	-2.61
NEW1	2.40	-2.52
NEW1	2.39	-2.54
NEW1	2.39	-2.61
NEW1	2.40	-2.42
NEW1	2.40	-2.43
NEW1	2.39	-2.51
NEW1	2.39	-2.38
NEW1	2.43	-2.41
NEW1	2.36	-2.41

NEW1	2.41	-2.48
NEW1	2.48	-2.38
NEW1	2.34	-2.40
NEW1	2.40	-2.38
NEW1	2.38	-2.53
NEW1	2.38	-2.43
NEW1	2.40	-2.40
NEW1	2.37	-2.33
NEW1	2.43	-2.72
NEW1	2.40	-2.34
NEW1	2.41	-2.67
NEW1	2.40	-2.58
NEW1	2.37	-2.34
NEW1	2.45	-2.50
NEW1	2.40	-2.61
NEW1	2.33	-2.49
NEW1	2.43	-2.45
NEW1	2.43	-2.36
NEW1	2.40	-2.31
NEW1	2.41	-2.32
NEW1	2.41	-2.25
NEW1	2.38	-2.40
NEW1	2.39	-2.53
NEW1	2.40	-2.43
NEW1	2.40	-2.58
NEW1	2.44	-2.59
NEW1	2.41	-2.49
NEW1	2.40	-2.48
NEW1	2.39	-2.53
NEW1	2.38	-2.52
NEW1	2.44	-2.61
NEW1	2.39	-2.26
NEW1	2.35	-2.64
NEW1	2.44	-2.50

NEW1	2.40	-2.54
NEW1	2.45	-2.41
NEW1	2.40	-2.43
NEW1	2.42	-2.49
NEW1	2.43	-2.28
NEW1	2.40	-2.48
NEW1	2.44	-2.46
NEW1	2.41	-2.33
NEW1	2.45	-2.63
NEW1	2.45	-2.41
NEW1	2.39	-2.47
NEW1	2.36	-2.33
NEW1	2.40	-2.56
NEW1	2.35	-2.37
NEW1	2.34	-2.55
NEW1	2.31	-2.61
STD DEV	0.03	0.10

Table 4: Standard errors for Batch 2

Name	C Corrected to VPDB	O Corrected to VPDB
NEW1	2.25	-2.64
NEW1	2.41	-2.46
NEW1	2.43	-2.50
NEW1	2.39	-2.50
NEW1	2.46	-2.32
NEW1	2.40	-2.40
NEW1	2.43	-2.37
NEW1	2.38	-2.45
NEW1	2.41	-2.48
NEW1	2.40	-2.52
NEW1	2.39	-2.63
NEW1	2.42	-2.46
NEW1	2.44	-2.34
NEW1	2.42	-2.51
NEW1	2.36	-2.30

NEW1	2.39	-2.45
NEW1	2.40	-2.61
NEW1	2.38	-2.46
NEW1	2.43	-2.46
NEW1	2.43	-2.40
NEW1	2.38	-2.40
STD DEV	0.04	0.09

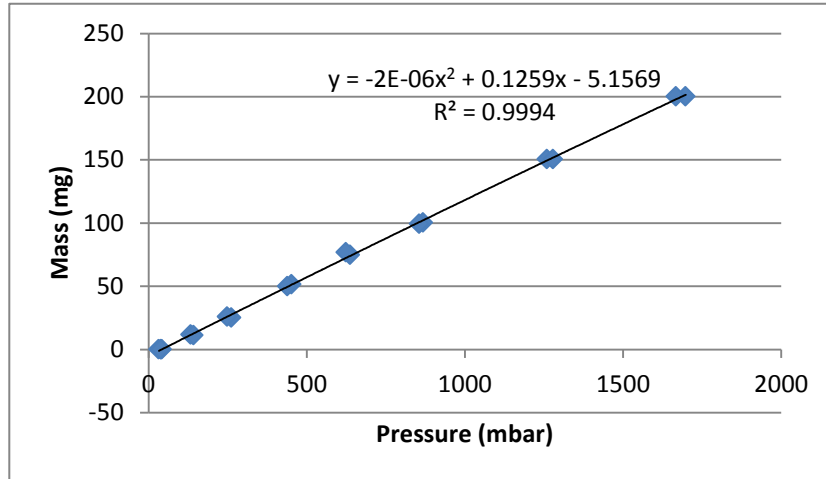
Table 5: Standard errors for Batch 3

Name	C Corrected to VPDB	O Corrected to VPDB
NEW1	2.41	-2.43
NEW1	2.49	-2.46
NEW1	2.43	-2.44
NEW1	2.36	-2.51
NEW1	2.40	-2.41
NEW1	2.38	-2.50
NEW1	2.39	-2.42
NEW1	2.35	-2.51
STD DEV	0.04	0.04

Pressure Calcimetry Results

Table 6: Pressure Calcimeter results for Bunkers Sandstone samples CK26.4.13 -67 to 70. Polynomial fit normalised is the % carbonate for the samples.

Vial #	Sample ID	Pressure (mbar)	Mass (mg)	Polynomial fit normalised
1	CaCO3	1698	200.04	101.4071646
2	CaCO3	1667	200.07	99.54547009
3	CaCO3	1259	150.37	99.87433531
4	CaCO3	1279	150.38	101.4746097
5	CaCO3	868	100.41	102.1984384
6	CaCO3	856	99.41	101.7483432
7	CaCO3	637	74.83	99.19799813
8	CaCO3	624	76.67	94.7253789
9	CaCO3	452	51.49	99.71119052
10	CaCO3	439	50.02	99.4157497
11	CaCO3	262	25.19	109.9309726
12	CaCO3	249	25.98	100.3394842
13	CaCO3	133	11.75	98.31848511
14	CaCO3	142	11.07	114.5489792
15	Blank	42	0	
16	Blank	39	0	
22	Blank	32	0	
23	Blank	39	0	
17	CK-67	87	201.68	2.866551964
18	CK-69	93	200.66	3.256504535
19	CK-68	61	199.06	1.263718477
20	CK-70	81	202.07	2.488186272
21	TG 833	61	201.75	1.246868897



Graph 1: Polynomial relationship of pressure and mass of the pressure calcimeter test.